Fully relativistic laser-induced ionization and recollision processes

Michael Klaiber,[1,2,*] Karen Z. Hatsagortsyan,[1,†] and Christoph H. Keitel[1,‡]
[1]*Max-Planck Institut für Kernphysik, Saupfercheckweg 1, D-69117 Heidelberg, Germany*
[2]*Theoretische Quantendynamik, Physikalisches Institut der Albert-Ludwigs-Universität, Hermann-Herder-Strasse 3, D-79104, Freiburg, Germany*

(Received 2 February 2007; revised manuscript received 4 April 2007; published 18 June 2007)

Relativistic above-threshold ionization (ATI) and high-harmonic generation in the long pulse regime are investigated via the Klein-Gordon equation employing the strong-field approximation. The energy and angular spectra of the rescattering electrons for ATI in the relativistic low frequency tunneling regime are examined. While the relativistic drift significantly reduces the rescattering efficiency in conventional sinusoidal laser waves, the employment of laser pulses specially tailored as a strong attosecond pulse train (APT) allows to counteract the drift. The optimal conditions for high-energy rescattering are found in relation to the duration of the attosecond pulse, to the time delay between pulses in the APT, as well as to the spectral content of the APT. The stability of the harmonic yield vs deformations of the tailored pulse shape is shown. The proposed method renders energies of more than 1 MeV possible for the rescattering atomic electron.

DOI: 10.1103/PhysRevA.75.063413 PACS number(s): 32.80.Rm, 32.80.Gc

I. INTRODUCTION

Above-threshold ionization (ATI) [1] and high-harmonic generation (HHG) [2] are phenomena which have been thoroughly investigated in the nonrelativistic regime, both experimentally and theoretically. The two processes are well understood within a three step model [3] where the ionized electron after propagation in the continuum by the laser field is driven back to the ionic core and scatters there in the case of ATI or recombines with emission of high harmonic radiation. The strong field approximation (SFA) [4], i.e., neglecting the influence of the Coulomb field of the residual atomic core on the ionized electron state and the influence of the laser field on the bound state, proved to be very successful for the description of atomic processes in strong laser fields. Further on, it has been developed into the quantum orbit method [5–7] that provides an intuitive description of strong-field processes. The relativistic theory of the SFA has been developed in [8] based on the Klein-Gordon equation and in [9] based on the Dirac equation and has been employed for the calculation of the relativistic direct ionization rate of hydrogen-like atoms in strong laser fields. The total transition rate, the photoelectron spectra and the angular distribution of the direct photoelectrons have been calculated in circularly [8–10] as well as in linearly [11] polarized strong laser fields. Spin effects in the direct ionization of an atom via the SFA based on the Dirac equation have been studied recently in [12]. In the relativistic theory of ionization there exists an exact solvable model; that is a Klein-Gordon particle in a short-range separable potential interacting with a circularly polarized strong laser field [13].

The application of the WKB approximation to the atomic ionization problem has resulted in the development of the imaginary-time-method [14]. It provides direct access to the asymptotics of the SFA theory and simple expressions for the direct ionization rates. The imaginary-time method has been extended to the relativistic regime in [15–17]. Relativistic theories of ATI of a quasiclassical nature have also been developed in [18–21]. In particular, simple analytical expressions for the angular and energy distribution of direct photoelectrons in the relativistic regime have been obtained in [19–21] by means of the adiabatic Landau-Dykhne approximation.

Numerical investigation of the strong field ionization in the relativistic regime encounters significant calculational difficulties at low frequencies of laser radiation but provides reliable results in the high frequency domain [22].

While the direct strong field ionization in the relativistic regime is a rather well investigated topic, the rescattering for ATI in the relativistic regime has not been thoroughly quantified. Particularly, the question of how the energy spectra and the angular distribution of the rescattered electron are modified in the relativistic regime still needs investigation. In the nonrelativistic regime where the laser magnetic field is negligible, the ionized electron is accelerated only in the laser polarization direction and is highly probable to return to the nucleus. In contrast, the relativistic regime is characterized by an additional force in the laser propagation direction due to the now non-negligible laser magnetic field. This is the reason for a drift of the electron in this direction after ionization and, consequently, a severe reducing of the rescattering probability [23–25]. It is therefore impossible to enter the hard x-ray regime of HHG by simply increasing the laser intensity. In order to avoid this problem, on the one hand, the properties of the atomic system can be modified by using atoms that move relativistically against the laser propagation direction [26], by employing positronium atoms instead of atoms [27], or antisymmetric molecular orbitals [28]. In the first case, the drift of the ionized electron is reduced by the increase of laser frequency in the system's center of mass. In the second, the electron's relativistic drift is compensated by an equally strong drift of the positron. In the last case, however, the compensation is due to the initial momentum of the tunneling electron from the antisymmetric orbital. On the

*Electronic address: klaiber@mpi-hd.mpg.de
†Electronic address: k.hatsagortsyan@mpi-hd.mpg.de
‡Electronic address: keitel@mpi-hd.mpg.de

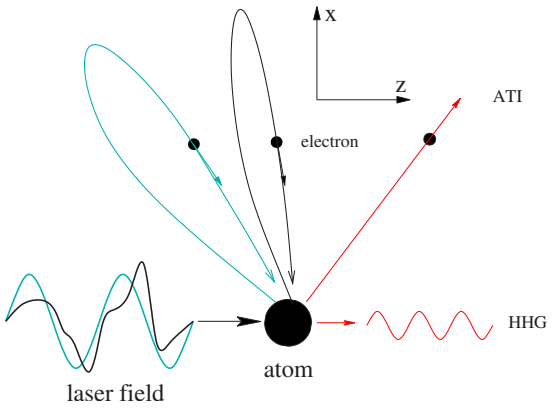

FIG. 1. (Color online) By employing specially tailored pulses instead of conventional sinusoidal ones, it is possible to reduce significantly the drift of the ionized electron due to the Lorentz force of the laser magnetic field. By this way, the rescattering probability can be increased by several orders of magnitude in the relativistic regime of laser atom interactions. x and z are the laser polarization and propagation direction, respectively.

other hand, the laser field can be modified to suppress the relativistic drift by using a tightly focused laser beam [29], two counterpropagating laser beams with linear [30,31] or equal-handed circular polarization [32], instead of one linearly polarized laser field. In the first case, the longitudinal field in the tightly focused laser beam counteracts the drift. In the second case, the Lorentz-force is eliminated only in a small area near the antinodes of the standing wave. In the third case however, it is eliminated over the whole focal region of the laser. In the weak relativistic regime where the relativistic drift velocity is not very high, the Lorentz force can also be compensated by a second weak laser beam which has polarization in the strong beam propagation direction [33]. By varying the time delay between the laser pulses, it is then possible to achieve a drift suppression for selected quantum orbits and an enhancement of the respective spectral region of HHG. As proposed in [34], pulses specially tailored as a strong attosecond pulse train (APT) instead of conventional sinusoidal laser pulses are employed, to suppress the relativistic drift of the ionized electron in the strong relativistic regime (see Fig. 1). The latter setup is investigated in detail later in this paper.

The SFA with the Schrödinger equation without the dipole approximation for the laser field has been developed [35] to investigate the weak relativistic regime of multiphoton ionization. The emergence of relativistic signatures in the recollision dynamics of the atomic electron in the weakly relativistic regime has been investigated for HHG in [23,33,36], as well as for ATI in [37], employing the SFA based on the Schrödinger equation with a multipole expansion of the laser-atom interaction Hamiltonian. HHG in the moderate relativistic regime has been calculated in [38] by the use of the relativistic SFA via the solution of the Klein-Gordon equation with a short range potential.

In this paper we investigate ATI and HHG in the relativistic regime. We examine the energy spectra and the angular distribution of the rescattered electron for ATI in the low frequency ($\omega \ll I_p$, where ω is the laser frequency, and I_p is the atomic ionization potential) tunneling regime in the case of a long laser pulse. The dependence of the cutoff energy for ATI or HHG on the emission direction and the laser intensity are analyzed. Detailed investigation is carried out on the ATI and HHG processes in specially tailored laser pulses in the form of an attosecond pulse train (APT). We investigate the dependence of the harmonic yield on the duration of the attosecond pulse in the train, on the time delay between the pulses in an APT, as well as on the spectral content of the APT. Analysis of the stability of the harmonic generation yield against deformations of the shape of the tailored pulse is carried out. As a result, we are able to formulate the APT parameter requirements for significant HHG in the MeV energy domain. In the calculation we employ the SFA to solve the Klein-Gordon equation, taking into account the rescattering as a perturbation. The probabilities of ATI and HHG are derived by the use of the saddle-point method for the calculation of the five-dimensional integral.

The plan of the paper is the following: Sec. II contains the presentation of the fully relativistic SFA theory for ATI. The photoelectron spectra and angular distribution for ATI are considered in Secs. II C and II D. HHG in the relativistic regime is considered in Sec. III. Section IV is dedicated to the analysis of ATI and HHG features in the tailored laser pulses. The conclusions are to be found in Sec. V.

II. ABOVE-THRESHOLD IONIZATION

A. SFA with the Klein-Gordon equation

We consider the ionization process of an atomic system by a linearly polarized plane laser field with polarization in x, magnetic field in y, and laser propagation in z directions for the relativistic parameter regime. Further, the single-active electron approximation [4] is applied, i.e., the interaction of the ionized electron with the ionic core plus bound electrons is represented by a static effective atomic potential. As spin effects have very little influence on the photoelectron spectra even in the strongly relativistic regime (see, e.g., Ref. [25]), we will resort to the Klein-Gordon equation for the description of the ATI dynamics in the relativistic regime (atomic units are used throughout this paper unless indicated otherwise),

$$[(i\partial^\mu + A^\mu/c + g^{\mu 0}V/c)^2 - c^2]\Psi(x) = 0, \tag{1}$$

where $\Psi(x)$ is the wave function of the active electron, $A^\mu = (0, \mathbf{A}(\eta))$ is the vector potential of the laser field in the radiation gauge (i.e., $\partial_\mu A^\mu = 0$), c is the speed of light, $x = (ct, x, y, z)$ is the time-space coordinate, $\eta = k^\mu x_\mu \equiv k \cdot x$ is the phase of the laser vector potential, $k^\mu = (\omega/c, 0, 0, k)$ is the wave vector, $\omega = ck$ is the angular frequency, and $g^{\mu\nu}$ is the metric tensor.

Equation (1) can be rewritten in the form

$$(\partial^\mu \partial_\mu + c^2)\Psi(x) = (V_L + V_{AI})\Psi(x) \tag{2}$$

with the electron-ion interaction operator

$$V_{AI} = 2iV/c^2\partial_t + V^2/c^2 \tag{3}$$

and the electron-field interaction operator

$$V_L = 2i\mathbf{A}(\eta)\cdot\boldsymbol{\nabla}/c - \mathbf{A}(\eta)^2/c^2. \tag{4}$$

The amplitude $M_{\mathbf{p}}$ for the ATI process yielding one electron with momentum $\mathbf{p}$ is given by

$$M_{\mathbf{p}} = \lim_{t\to\infty}(\Psi_{\mathbf{p}}^f, \Psi), \tag{5}$$

where $\Psi_{\mathbf{p}}^f(x)$ are the reference states represented by the continuum states of the Klein-Gordon equation in the atomic potential which have an asymptotic momentum $\mathbf{p}$ at $t\to\infty$; the Klein-Gordon scalar product is defined by $(f,g) = \int d^3x f^*(x)(i\overleftrightarrow{\partial}_{ct} - 2V/c)g(x)$ [39].

The Lippmann-Schwinger equation with regard to the electron-field interaction V_L for the wave function $\Psi(x)$ is given by

$$\Psi(x) = \Phi(x) + \int d^4x' G(x,x')V_L(x')\Phi(x'). \tag{6}$$

$\Psi(x)$ satisfies the boundary condition $\lim_{t\to-\infty}\Psi = \Phi$, where Φ is the initial bound state of the atom. It is an eigenstate of the energy operator in the radiation gauge [40] and can be approximated by

$$\Phi(x) = \frac{\phi_0(\mathbf{x})\sqrt{c}}{\sqrt{2(c^2 - I_p)}}\exp\{-i[(c^2 - I_p)t + \mathbf{x}\cdot\mathbf{A}/c]\} \tag{7}$$

with the nonrelativistic ground state wave function ϕ_0. The use of the nonrelativistic wave function for the bound state is justified for the following reason: we consider laser intensities up to $I = 10^{20}$ W/cm^2, correspondingly, the ionization potential of the active atomic electron (I_p) must be large enough to avoid over-the-barrier ionization [25],

$$I_p[\mathrm{eV}] > \left(\frac{2I\,[\mathrm{W/cm^2}]}{10^{11}}\right)^{1/3}, \tag{8}$$

but also close to the threshold value, in order to have a significant ionization probability in the tunneling regime. The domain of the latter regime is known to be at a small Keldysh parameter $\gamma = \sqrt{I_p/2U_p} < 1$, where $U_p = E_0^2/4\omega^2$ is the ponderomotive potential, and the amplitude of the laser electric field E_0. The above-mentioned conditions require an ionization potential up to $I_p \approx 2$ keV, with the presumption that the bound dynamics of the active electron is still nonrelativistic, $I_p \ll c^2$. A more precise condition for the nonrelativistic tunneling dynamics is given by Eq. (23) in [16] which estimates the ratio of the nonrelativistic tunneling probability to the relativistic one,

$$w_{NR}/w_R \approx \exp\{-[(Z\alpha)^5/36]\sqrt{I_{cr}/I}\}, \tag{9}$$

where $I_{cr} = 2.3\times10^{29}$ W/cm^2 is the intensity of the Schwinger critical field, Z is the charge of a hydrogen-like ion, $I_p = c^2[1 - \sqrt{1-(Z\alpha)^2}]$, and α is the fine structure constant. This formula shows that at a laser field intensity of 10^{20} W/cm^2, relativistic effects in the tunneling dynamics are not significant up to $Z\alpha \approx 0.15$, which corresponds to $I_p \approx 5$ keV (see also Fig. 1 in [17]).

$G(x,x')$ in Eq. (6) is the positive energy Green function of the Klein-Gordon equation (1). Its Lippmann-Schwinger equation with respect to the electron-ion interaction reads

$$G(x,x') = G^V(x,x') + \int d^4x''\, G(x,x'')V_{AI}(x'')G^V(x'',x') \tag{10}$$

with the Volkov Green function of the Klein-Gordon equation in the laser field $G^V(x,x')$ given in [38]

$$G^V(x,x') = -i\theta(t-t')\int \frac{c\,d^3\mathbf{q}}{2\varepsilon_{\mathbf{q}}(2\pi)^3}\exp\left[-iq\cdot(x-x') - i\int_{\eta'}^{\eta} d\tilde{\eta}\left(\frac{[\mathbf{q} + \mathbf{A}(\tilde{\eta})/2c]\cdot\mathbf{A}(\tilde{\eta})/c}{k\cdot q}\right)\right] \tag{11}$$

and the energy momentum $q = (\varepsilon_{\mathbf{q}}/c, \mathbf{q})$, and $\varepsilon_{\mathbf{q}} = \sqrt{c^2\mathbf{q}^2 + c^4}$. The insertion of Eq. (10) in Eq. (6) yields

$$\Psi(x) = \Phi(x) + \int d^4x'\, G^V(x,x')V_L(x')\Phi(x') + \int d^4x' \int d^4x''[G(x,x'')V_{AI}(x'') \times G^V(x'',x')V_L(x')\Phi(x')], \tag{12}$$

which is still exact. Along the lines of the SFA, the influence of the atomic potential on the ionized electron can be considered small compared to the one of the laser field. Then, the atomic potential in the final reference states can be neglected, and the substitution $G \to G^V$ can be made which includes maximally one contact interaction of the revisiting electron with the ionic core.

Consequently, the amplitude of ATI is then given by

$$M_{\mathbf{p}} = -i\int d^4x'\, \Psi_{\mathbf{p}}^V(x')^* V_L(x')\Phi(x') - i\int d^4x' \int d^4x''[\Psi_{\mathbf{p}}^V(x')^* V_{AI}(x') \times G^V(x',x'')V_L(x'')\Phi(x'')], \tag{13}$$

where $\Psi_{\mathbf{p}}^V(x)$ is the Klein-Gordon Volkov state which describes the electron in the laser field in the radiation gauge [8],

$$\Psi_{\mathbf{p}}^V(x) = \frac{\sqrt{c}}{\sqrt{2(2\pi)^3\varepsilon_{\mathbf{p}}}}\exp\left(-ip\cdot x + i\int_{\eta}^{\infty} d\tilde{\eta}\frac{[\mathbf{p} + \mathbf{A}(\tilde{\eta})/2c]\cdot\mathbf{A}(\tilde{\eta})/c}{k\cdot p}\right), \tag{14}$$

satisfying the boundary condition that when the laser field is switched off at $t\to\infty$ the electron has an asymptotic momentum $\mathbf{p}$. The first term in Eq. (13) describes direct ionization within the SFA, whereas the second includes rescattering at the ionic core. Analogous to the nonrelativistic case [6], we can use the identity $V_L = -\partial_\mu\partial^\mu + V_L + \partial_\mu\partial^\mu - V_{AI} + V_{AI}$ and derive for the amplitude

$$M_{\mathbf{p}} = -i \int d^4x' \, \Psi_{\mathbf{p}}^V(x')^* V_{AI}(x') \Phi(x')$$
$$- i \int d^4x' \int d^4x'' [\Psi_{\mathbf{p}}^V(x')^* V_{AI}(x')$$
$$\times G^V(x',x'') V_{AI}(x'') \Phi(x'')]. \quad (15)$$

Now we apply the integration variable transformation $(ct',\mathbf{x}') \rightarrow (\eta',\mathbf{x}')$ and $(ct'',\mathbf{x}'') \rightarrow (\eta'',\mathbf{x}'')$ with $\eta' = k^\mu x'_\mu$ and $\eta'' = k^\mu x''_\mu$. Assuming that the laser wavelength is much larger than the spatial extension of the wave packet of the ionized electron, the momentum amplitude of ATI can then be written as

$$M_{\mathbf{p}} \equiv -i \int_{-\infty}^{\infty} d\eta' \, m(\mathbf{p},\eta') \exp[i(\varepsilon_{\mathbf{p}} + I_p - c^2)\eta'/\omega]$$
$$= \lim_{\eta\to\infty} \Bigg(-i \int_{-\infty}^{\infty} d\eta' \, m^D(\mathbf{p},\eta') \exp[-iS(\mathbf{p},\eta,\eta')]$$
$$- i \int_{-\infty}^{\infty} d\eta' \int_{-\infty}^{\eta'} d\eta'' \int d^3\mathbf{q} \, m^R(\mathbf{p},\mathbf{q},\eta',\eta'')$$
$$\times \exp\{-i[S(\mathbf{p},\eta,\eta') + S(\mathbf{q},\eta',\eta'')]\} \Bigg) \quad (16)$$

with the matrix element in the SFA,

$$m^D(\mathbf{p},\eta) = \sqrt{\frac{c^2 - I_p}{\varepsilon_{\mathbf{p}}}} \frac{\left\langle \mathbf{p} + \frac{\mathbf{A}(\eta')}{c} - \frac{\mathbf{k}}{\omega}(\varepsilon_{\mathbf{p}} + I_p - c^2) | V | 0 \right\rangle}{\omega}, \quad (17)$$

and the rescattering matrix element,

$$m^R(\mathbf{p},\mathbf{q},\eta',\eta'') = \sqrt{\frac{c^2 - I_p}{\varepsilon_{\mathbf{p}}}} \frac{\tilde{\varepsilon}_{\mathbf{q}}(\eta')}{\varepsilon_{\mathbf{q}}} \left\langle \mathbf{p} - \frac{\varepsilon_{\mathbf{p}}}{\omega}\mathbf{k} | V | \mathbf{q} - \frac{\varepsilon_{\mathbf{q}}}{\omega}\mathbf{k} \right\rangle$$
$$\times \frac{\left\langle \mathbf{q} + \frac{\mathbf{A}(\eta')}{c} - \frac{\mathbf{k}}{\omega}(\varepsilon_{\mathbf{q}} + I_p - c^2) | V | 0 \right\rangle}{\omega^2}, \quad (18)$$

where $\langle \mathbf{p}|V|\mathbf{q}\rangle$ and $\langle \mathbf{p}|V|0\rangle$ are the matrix elements of the atomic potential. $S(\mathbf{p},\eta,\eta') = \int_{\eta'}^{\eta} d\tilde{\eta} [\tilde{\varepsilon}_{\mathbf{p}}(\tilde{\eta}) - c^2 + I_p]/\omega$ is the quasiclassical action and the relativistic energy of the electron in the laser field is given by

$$\tilde{\varepsilon}_{\mathbf{p}}(\eta) = \varepsilon_{\mathbf{p}} + \frac{\omega}{k\cdot p}[\mathbf{p} + \mathbf{A}(\eta)/2c] \cdot \mathbf{A}(\eta)/c. \quad (19)$$

Further, we explicitly take into account that the ATI process in a long laser pulse is a periodic one which results in a discrete photoelectron spectrum. Thus, the integrand $m(\mathbf{p},\eta')$ in the amplitude expression of Eq. (16) is periodic and can be expanded in a Fourier series $m(\mathbf{p},\eta') = \sum_n m_n(\mathbf{p}) \exp(-in\eta')$. Then, the fully differential ionization rate is given by the following expression [42]:

$$dw_{\mathbf{p}} = 2\pi \sum_n |m_n(\mathbf{p})|^2 \omega^2 \delta(\varepsilon_{\mathbf{p}} + I_p - c^2 - n\omega) d^3p, \quad (20)$$

which yields the angular resolved photoelectron spectrum,

$$\frac{dw_{\mathbf{p}}}{d\Omega} = 2\pi\omega^2 \frac{p\varepsilon_{\mathbf{p}}}{c^2} |m_{\mathbf{p}}|^2, \quad (21)$$

with the differential solid angle $d\Omega$ and

$$m_{\mathbf{p}} = \lim_{\eta\to\infty} \frac{1}{2\pi} \Bigg(\int_{-\pi}^{\pi} d\eta' \, m^D(\mathbf{p},\eta') \exp[-iS(\mathbf{p},\eta,\eta')]$$
$$+ \int_{-\pi}^{\pi} d\eta' \int_{-\infty}^{\eta'} d\eta'' \int d^3\mathbf{q} \, m^R(\mathbf{p},\mathbf{q},\eta',\eta'')$$
$$\times \exp\{-i[S(\mathbf{p},\eta,\eta') + S(\mathbf{q},\eta',\eta'')]\} \Bigg). \quad (22)$$

B. The long wavelength regime

In the long wavelength regime $(U_p \gg I_p \gg \omega)$ the one-dimensional integral in the first term of Eq. (16) as well as the fivefold integral in the second term can be carried out by the saddle-point method. The saddle-point conditions are $\partial_{\eta'} S(\mathbf{p},\eta,\tilde{\eta}') = 0$ and $\partial_i [S(\tilde{\mathbf{q}},\tilde{\eta}',\tilde{\eta}'') + S(\mathbf{p},\eta,\tilde{\eta}')] = 0$ with $i \in \{\mathbf{q},\eta',\eta''\}$, respectively. The saddle point for direct ionization is then defined via

$$\tilde{\varepsilon}_{\mathbf{p}}(\tilde{\eta}') = c^2 - I_p, \quad (23)$$

where $\mathbf{p}$ is the momentum of the ionized electron and $\tilde{\eta}'$ the ionization phase. In the case of rescattering we obtain

$$\tilde{q}_x = -\frac{\int_{\tilde{\eta}''}^{\tilde{\eta}'} d\tilde{\eta} \, A(\tilde{\eta})/c}{\tilde{\eta}' - \tilde{\eta}''},$$

$$\tilde{q}_y = 0,$$

$$\tilde{q}_z = \frac{\tilde{q}_x^2 + q_m^2/2}{\sqrt{c^2 - q_m^2 - \tilde{q}_x^2}},$$

$$\tilde{\varepsilon}_{\mathbf{p}}(\tilde{\eta}') = \tilde{\varepsilon}_{\tilde{\mathbf{q}}}(\tilde{\eta}'),$$

$$\tilde{\varepsilon}_{\tilde{\mathbf{q}}}(\tilde{\eta}'') = c^2 - I_p, \quad (24)$$

where $\tilde{\mathbf{q}} = \tilde{\mathbf{q}}(\tilde{\eta}',\tilde{\eta}'') = (\tilde{q}_x,\tilde{q}_y,\tilde{q}_z)$ is the drift momentum of the ionized electron in the first step, $q_m^2 = -\int_{\tilde{\eta}''}^{\tilde{\eta}'} d\tilde{\eta} \, \mathbf{A}(\tilde{\eta})^2/[c^2(\tilde{\eta}' - \tilde{\eta}'')]$, and $\tilde{\eta}''$, $\tilde{\eta}'$ the ionization and rescattering phases, respectively. Using the solutions of Eqs. (23) and (24), the momentum amplitude can be written as

$$m_{\mathbf{p}} = \frac{1}{2\pi} \lim_{\eta\to\infty} \sum_{SP} \left(\sqrt{\frac{2\pi i}{\partial_{\eta',\eta'} S(\mathbf{p},\eta,\hat{\eta}')}} \times m^D(\mathbf{p},\hat{\eta}') \exp[-iS(\mathbf{p},\eta,\hat{\eta}')] + \sqrt{\frac{(2\pi i)^5}{\det[\partial_{ij} S(\tilde{\mathbf{q}},\tilde{\eta}',\tilde{\eta}'') + \partial_{ij} S(\mathbf{p},\eta,\tilde{\eta}')]}} \times m^R(\mathbf{p},\tilde{\mathbf{q}},\tilde{\eta}',\tilde{\eta}'') \exp\{-i[S(\tilde{\mathbf{q}},\tilde{\eta}',\tilde{\eta}) + S(\mathbf{p},\eta,\tilde{\eta}')]\} \right), \tag{25}$$

where *SP* indicates summation over all saddle points. In the calculation of the matrix elements in Eqs. (17) and (18) we assume that V is a zero-range potential [41]

$$V = \frac{2\pi}{\kappa} \delta(\mathbf{r}) \partial_r r \tag{26}$$

with its ground state wave function in the momentum space

$$\tilde{\phi}_0(\mathbf{p}) = \frac{\sqrt{\kappa}/\pi}{\kappa^2 + p^2} \tag{27}$$

and its matrix elements

$$\langle \mathbf{p}|V|0\rangle = -\frac{\sqrt{\kappa}}{2\pi},$$

$$\langle \mathbf{p}|V|\mathbf{q}\rangle = 1/4\pi^2\kappa, \tag{28}$$

with $\kappa = \sqrt{2I_p}$. By using the physically relevant saddle points [6], the process amplitude $m_{\mathbf{p}}$ is calculated.

C. Low-energy spectra and angular distribution of direct electrons for ATI

We now discuss the photoelectron energy spectra and angular distribution including rescattering in the relativistic regime.

In the nonrelativistic case the photoelectron energy spectrum consists of a considerably decreasing low-energy part up to approximately $2U_p$, resulting from direct ionized electrons and a long plateau region with a characteristic cutoff at high energies up to approximately $10U_p$ arising from rescattered electrons [6]. In the relativistic case we will identify several changes.

Our focus of interest is on the rescattering features in the relativistic regime. To obtain non-negligible rescattering probabilities, we choose the *moderately* relativistic regime, employing a laser with an average intensity of $I = 1.8 \times 10^{17}$ W/cm^2 at an angular frequency of $\omega = 0.05$ a.u. equals a suboptical wavelength of $\lambda = 911$ nm. In fact, the relativistic parameter of the laser field in this case is smaller than 1, $a_0 \equiv E_0/c\omega = 0.33$. We apply a long laser pulse with an electric field $\mathbf{E}(\eta) = \mathbf{e}_x E_0(\eta)\sin\eta$ that is adiabatically turned on and off. We consider the tunneling regime of ionization close to the over-the-barrier ionization limit to have significant ionization probabilities, i.e., at a given high laser intensity, the ionization potential should be high enough to be close to the threshold value of Eq. (8), and exceeds it only slightly.

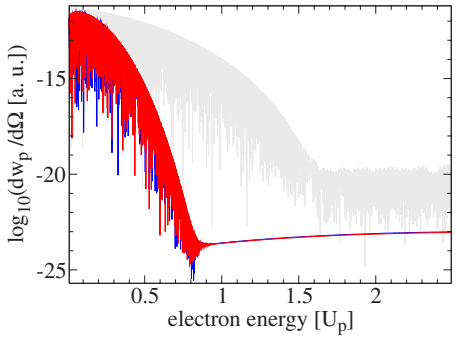

FIG. 2. (Color online) Low-energy photoelectron spectrum in a laser field with angular frequency $\omega = 0.05$ a.u. and intensity $I = 1.8 \times 10^{17}$ W/cm^2 (the laser electric field strength is 2.24 a.u.) via $\log_{10}(dw_{\mathbf{p}}/d\Omega)$ in Eq. (21), with final electron momentum in the polarization direction. The model potential is adapted to Be^{3+} with an ionization potential of $I_p = 8$ a.u. The electron energy is scaled in multiples of U_p: (gray) within the dipole approximation, (blue, the darkest) with leading magnetic field and relativistic corrections [37], (red) Klein-Gordon equation.

First, we shortly discuss some features of direct ionization, calculating the low-energy photoelectron spectrum and the angular distribution of the electrons. The full relativistic calculations via the Klein-Gordon equation are compared with the results of the weak relativistic theory via the Schrödinger equation including leading nondipole and relativistic corrections [37] to clarify the extent of the applicability of this approximate approach.

Figure 2 shows the low-energy part for electrons emitted in the laser polarization direction. The calculations based on the Klein-Gordon equation are compared with the dipole as well as with the weak relativistic approximation. As one can see, the ionization rate decreases faster in the relativistic treatment and the plateau starts at lower energies. The reason for this is that in the relativistic regime the electron emission direction is shifted along the laser propagation direction because of the drift of the ionized electrons induced by the Lorentz force. As a result, the ionization yield in polarization direction is smaller and becomes less important. Furthermore, the spectrum including only leading nondipole corrections is nearly correct since the ratio of the electron velocity to the speed of light is not negligible yet still small for direct ionization.

In Fig. 3 the energy and angular resolved spectrum for direct ionized electrons in the chosen moderately relativistic regime is displayed. One can see that in the nonrelativistic description the distribution is symmetric with respect to the emission angle. The emission occurs mainly in the polarization direction and the emission for small energies is favored. Due to the adequate relativistic description of the process, the distribution is shifted in the laser propagation direction and becomes asymmetric. However, the width of the energy and angular distribution remains the same as in the nonrelativistic case, as long as the momentum spreading due to the field remains nonrelativistic, $\delta p_E = \sqrt{3\omega/\gamma^3} \ll c$ [20]. In the tunneling regime this condition [at the threshold defined by

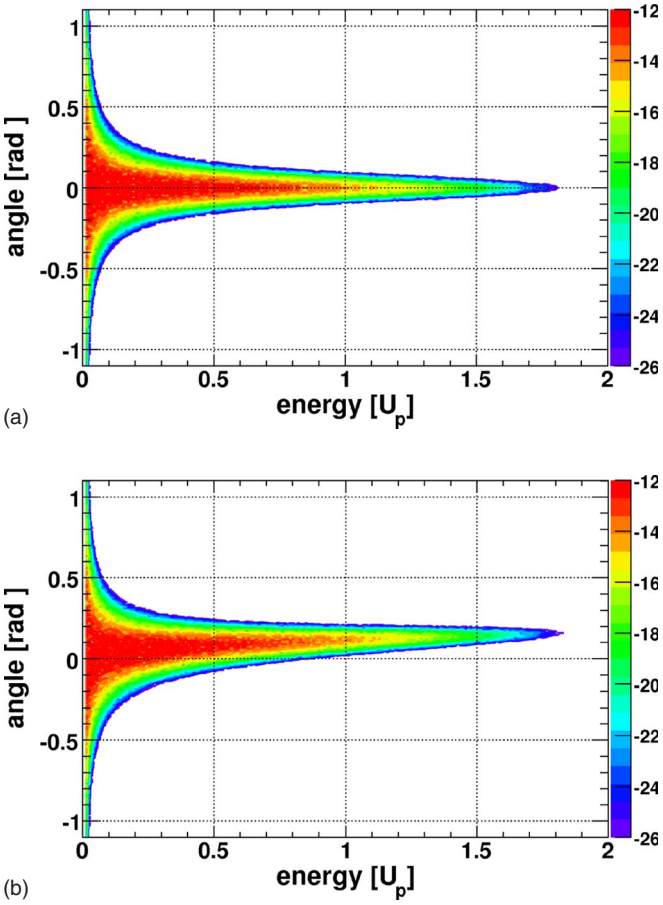

FIG. 3. (Color online) Spectrum of the direct ionized electron in dependence of the final energy in units of U_p and the emission angles θ, $\phi=0$, via $\log_{10}(dw_{\mathbf{p}}/d\Omega)$ in Eq. (21): (a) within the dipole approximation; (b) Klein-Gordon equation. The parameters of the driving laser field as well as of the atom are the same as in Fig. 2.

Eq. (8)] is violated only at rather high laser intensities with $a_0>3$. Further, the drift of the ionized electron in the laser propagation direction is larger than expected for higher energies, see e.g., Ref. [19].

The emission rate integrated over all directions defines the probability of an atom emitting an electron with a given final energy ε per unit time,

$$w_\varepsilon = \int \frac{dw_{\mathbf{p}}}{d\Omega} d\Omega. \tag{29}$$

The low-energy spectrum of electrons integrated over all emission directions is shown in Fig. 4. There it can be seen that the total rates of emitting an electron with a certain energy are nearly equal for the different approximations as long as direct ionization dominates. This is because the amount of the wave packet that tunnels out of the barrier is the same in all approximations, since in the case considered here relativistic corrections to the bound state dynamics of the electron in the atom are negligible [see Eq. (9) and the discussion afterwards] and are not taken into account in all three cases. Only the following action of the laser field after ionization that is considered with a different accuracy in the

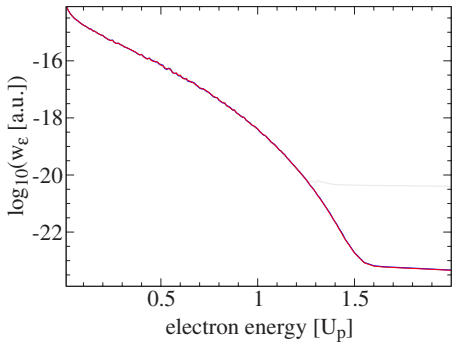

FIG. 4. (Color online) Low-energy photoelectron spectrum via $\log_{10}(w_\varepsilon)$ in Eq. (29), integrated over all emission angles. The parameters of the driving laser field as well as of the atom are the same as in Fig. 2. The electron energy is scaled in multiples of U_p: (gray) within the dipole approximation, (blue) with leading magnetic field and relativistic corrections [37], (red) Klein-Gordon equation (the red and blue curves coincide).

different approximations, yields different angular distributions; however, it leaves the total rate of direct ionization unchanged. The mismatch between the dipole and the relativistic results at higher energies, larger than $1.5U_p$, is due to rescattering which we consider in the next section.

D. High-energy spectra and angular distribution for ATI

The discrepancy between the results of the relativistic and the nonrelativistic (dipole approximation) consideration becomes prominent in those cases where rescattering plays a role.

Figure 5 displays the high-energy part of the electrons emitted in the direction of the maximal cutoff energy. We point out the following characteristic features of these spectra. First, the relativistic treatment of ATI leads to a lowering of the plateau. Since the ionized electron experiences a drift

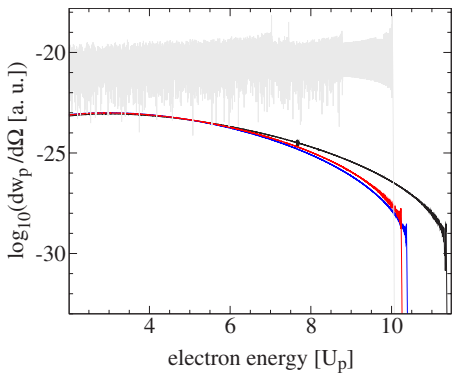

FIG. 5. (Color online) Photoelectron spectrum via $\log_{10}(dw_{\mathbf{p}}/d\Omega)$ in Eq. (21), with final electron momentum in direction of the maximal cutoff energy. The parameters of the driving laser field as well as of the atom are the same as in Fig. 2. The electron energy is scaled in multiples of U_p: (gray, the first from top) within the dipole approximation, (black, second) with leading magnetic field corrections, (red, third) Klein-Gordon equation, (blue, fourth) with leading magnetic field and relativistic corrections [37].

induced by the Lorentz force in the laser propagation direction, it can only rescatter with the ionic core when it starts with a nonvanishing negative velocity in this direction. Since the tunneling with nonzero velocity is significantly less probable than with zero velocity, the ionization probability for electrons that rescatter is smaller than in the nonrelativistic case. The probability in the case shown in Fig. 5 is decreased by three orders of magnitude for low final energies and nearly 10 orders of magnitude for high energies, in comparison to the situation when the electron starts with zero velocity.

Second, the strongly fluctuating spectrum in the dipole approximation resulting from interference of at least two quasiclassically possible trajectories of the ionized electron, vanishes in the relativistic case. This is because of the fact that the contribution of longer duration trajectories becomes negligible due to quantum spreading, on the one hand, and the relativistic drift, on the other hand. The latter can be explained as follows. For a long trajectory, the time span where the laser magnetic field impact on the ionized electron dynamics is essential, is larger than for a short trajectory. As a result, the relativistic drift for the long trajectory is larger than for the short one. Therefore, a larger initial momentum is required to prevent the drift for the long trajectory than for the short one which results in a larger difference in the ionization probabilities of the different trajectories. For the same reasons, the multiplateau structure also vanishes for a relativistic laser intensity and only the saddle point with the shortest travel time is responsible for the spectrum.

Further, the plateau is no longer flat, but bended. The bend increases with increasing laser intensity as the rescattering electrons with higher energies move on average with higher velocity and thus experience a higher Lorentz-force induced drift, yielding a lower recombination probability.

Finally one can observe the shifting of the cutoff energy of the electron spectrum to higher energies. While all modifications of the ATI process listed above are mostly attributed to the laser magnetic field, the last one is also influenced by the relativistic mass shift. This is displayed in the spectrum obtained by including only the leading order correction from the laser magnetic field (see also Sec. II E).

The spectrum that includes only nondipole and relativistic corrections is qualitatively right, and is quantitatively correct up to final electron energies of $7U_p$ (equal to 87.5 keV in the considered case of $U_p=12.5$ keV). Next to leading order corrections for the laser magnetic field and relativistic mass shift effects become especially important near the cutoff of the spectrum. They are responsible for the emission rate increase, and the cutoff value decrease. The role of relativistic effects in the strong field ionization processes can be described by the following parameters [37]: $\eta=(E_a/E)p_{z0}^2/2I_p=\sqrt{2I_p}ca_0^3/\omega$ and a_0^2, where p_{z0} is the initial momentum of the ionized electron allowing rescattering, E_a and E are the atomic and the laser field, respectively. The parameter η describes the influence of the magnetic field induced drift which is responsible for the dramatic damping of the plateau. In the considered moderate relativistic regime (a laser angular frequency of 0.05 a.u., a laser intensity of 10^{17} W/cm^2, $a_0\sim 0.33$, and an atom ionization potential of 8 a.u.) $\eta\sim 10^2$ indicates that the ionization process followed by rescattering is strongly suppressed. The weak relativistic theory with nondipole corrections includes the drift effect and describes it properly (see Fig. 5). The parameter a_0^2 describes the influence of the relativistic mass shift as well as, that of the laser magnetic field on the energy gain by the electron. In the considered regime $a_0^2\approx 0.1$ is rather small. That is why the weak relativistic theory containing the leading relativistic mass shift correction describes the process satisfactorily up to laser intensities of 10^{17} W/cm^2. For higher laser intensities with $a_0^2>0.1$, corrections next to the leading order in the laser magnetic field and in the relativistic mass shift become important, too, and are responsible for a decrease in the cutoff and an increase in the emission rate at high energies of the ionized electron.

Relativistic signatures for the rescattered electrons are also conspicuous in their angular distribution. One might expect that the relativistic drift tilts the angular distribution in the laser propagation direction. In fact, the classical relativistic equations of motion indicate the qualitative behavior of the angular distribution of the rescattered electrons. Thus, the electron energy and momenta, after the rescattering at the moment η_0, are (see, e.g., Ref. [43])

$$p_x = A(\eta)/c - A(\eta_0)/c + p_{x0},$$

$$p_z = \frac{[A(\eta)/c - A(\eta_0)/c + p_{x0}]^2 - p_{x0}^2}{2\Lambda} + p_{z0},$$

$$\varepsilon_{\mathbf{p}} = c\frac{[A(\eta)/c - A(\eta_0)/c + p_{x0}]^2 - p_{x0}^2}{2\Lambda} + \varepsilon_0, \tag{30}$$

where $\varepsilon_0, \mathbf{p}_0$ are the energy and momentum of the electron immediately after the rescattering, $\Lambda=\Lambda(p_x,p_z)=\varepsilon_{\mathbf{p}}/c-p_z$ the integral of motion. After the interaction the electron energy and momenta are

$$p_x = p_{x0} - A(\eta_0)/c,$$

$$p_z = \frac{[p_{x0} - A(\eta_0)/c]^2 - p_{x0}^2}{2\Lambda} + p_{z0},$$

$$\varepsilon_{\mathbf{p}} = c\frac{[p_{x0} - A(\eta_0)/c]^2 - p_{x0}^2}{2\Lambda} + \varepsilon_0. \tag{31}$$

Let us estimate the maximal rescattering angle at a given final electron energy $\varepsilon_{\mathbf{p}}=\epsilon U_p=\epsilon c^2 a_0^2/4$. The rescattering angle will be maximal at a given final electron energy when the recolliding electron has the maximal energy $\varepsilon_0=U_p^{\max}\approx 3U_p=3c^2a_0^2/4$. Then, the field is minimal at the electron recollision moment, i.e., $A(\eta_0)=-a_0c^2$. Thus, we have

$$p_x = p_{x0} + a_0 c,$$

$$p_z = \frac{\epsilon - 3}{4}a_0^2 c + p_{z0}, \tag{32}$$

and the maximal rescattering angle with respect to the polarization direction is determined from the following equation:

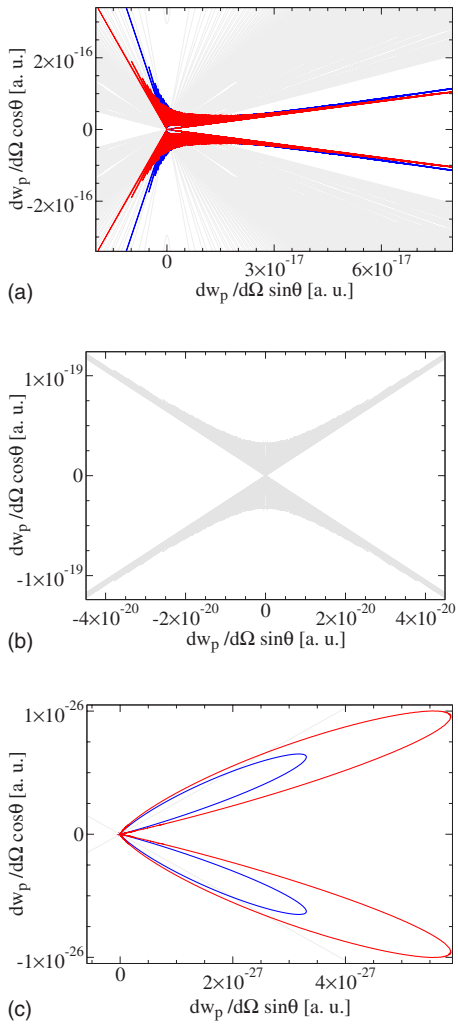

FIG. 6. (Color online) Polar plots of the angular distribution for a final electron energy of $9U_p$, (a) with an laser intensity of 7×10^{16} W/cm^2, an angular frequency of $\omega=0.05$ a.u. (equal to $U_p=200$ a.u.), and an ionization potential of $I_p=4$ a.u., (b) and (c) with parameters as in Fig. 2: (gray) within the dipole approximation, (blue, the darkest) with magnetic field corrections and the relativistic mass shift, (red) Klein-Gordon equation. $\theta=0$ corresponds to the direction of the laser polarization.

$$\cos\theta + \frac{\epsilon-3}{4}a_0 \sin\theta = \frac{\sqrt{2}}{\sqrt{\epsilon}}\frac{\epsilon-1+\epsilon(\epsilon-3)a_0^2/4}{4\sqrt{1+\epsilon a_0^2/8}}. \quad (33)$$

In the nonrelativistic case (dipole approximation) $a_0 \to 0$, there are two symmetric solutions of Eq. (33) $\theta=\pm\theta_d$ corresponding to two possible symmetric values for p_z [additionally, the angular distribution is symmetric with respect to the propagation axis, because of the symmetry with respect to the $p_x \to -p_x$, $A(\eta_0) \to -A(\eta_0)$ transformation]. According to Eq. (33) in the relativistic case $\theta=\pm\theta_d+\delta$, i.e., the maximal electron emission angle at the rescattering is tilted in the laser propagation direction (see also Sec. II E). In the weak relativistic regime $a_0 \ll 1$, $\delta \approx (\epsilon-3)a_0/4$.

Figure 6 displays the polar plot of the photoelectron angular distribution with the final electron energy of $9U_p$ within the dipole approximation, including nondipole and relativistic corrections and based on the Klein-Gordon equation for a relativistic field parameter of $a_0 \sim 0.21$ and $a_0 \sim 0.33$, respectively. Due to the linear scale of the representation, the huge difference in the emission rate is visible and of course larger for a stronger driving laser field. The drift of the emitted electrons in the propagation direction of the laser is clearly displayed. Furthermore, the characteristic side lobes as a result of the rate increase near the cutoff energy is shifted in the laser propagation direction for the smaller field, whereas they vanish as well as the interference pattern in the stronger field. Again, we observe that the spectrum with nondipole and relativistic corrections is qualitatively correct, but not quantitatively.

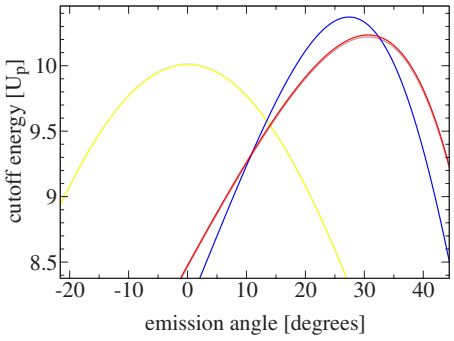

FIG. 7. (Color online) Cutoff energy scaled in multiples of U_p against the emission angle $\theta=\arctan(p_z/p_x)$: (blue, the first from top) with magnetic field corrections and the relativistic mass shift, (red, second) Klein-Gordon equation, (brown, second) classical relativistic coinciding with the red curve, (yellow, third) classical nonrelativistic, (gray, third) within the dipole approximation coinciding with the classical nonrelativistic curve. The parameters of the driving laser field as well as of the atom are the same as in Fig. 2 ($U_p=500$ a.u.).

E. The cutoff energy

Relativistic signatures are also seen in the cutoff energy of ATI electron spectra. The final electron energy after ionization is

$$\varepsilon^F = \lim_{\eta\to\infty} \tilde{\varepsilon}_{\mathbf{p}}(\eta) \quad (34)$$

when the laser field is switched off, $\mathbf{A}(\infty)=0$. The cutoff energy is now defined by Eqs. (24) and the additional condition

$$\lim_{\eta\to\infty} d\tilde{\varepsilon}_{\mathbf{p}}(\eta)/d\eta' = 0. \quad (35)$$

Due to the relativistic effects, the angular distribution of the electron is altered and the cutoff energy depends on the electron emission direction. Figure 7 displays the dependence of the cutoff energy on the emission angle of the electron in the moderately relativistic regime ($U_p=500$ a.u.) and using different approximations. The Lorentz-force induced drift is the reason for the shift of the maximal cutoff energy in the laser propagation direction. This also explains why the angular distribution of the electron with a certain energy is tilted in the laser propagation direction, e.g., the electrons

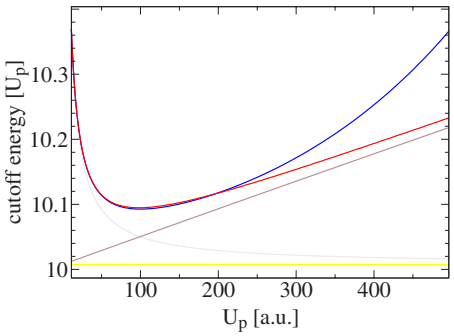

FIG. 8. (Color online) Maximal cutoff energy scaled in multiples of U_p against the laser intensity represented by U_p: (blue, the first from top) with magnetic field corrections and the relativistic mass shift, (red, second) Klein-Gordon equation, (brown, third) classical relativistic, (gray, fourth) within the dipole approximation, (yellow, fifth) classical nonrelativistic. The parameters of the driving laser field as well as of the atom are the same as in Fig. 2.

with an energy of $9U_p$ are distributed within the angular region of 10 up to 45 degrees. Further, the cutoff energy is slightly higher than in the nonrelativistic case since the electron sees the laser field redshifted due to the relativistic drift. The latter increases the coherent interaction time of the electron with the laser field and, consequently, the energy acquired by the electron from the laser field. The calculations including leading nondipole and relativistic corrections overestimate this effect, but are qualitatively correct. Furthermore, the classical calculation of the cutoff energy coincides with quantum results in the nonrelativistic as well as in the relativistic case. In the classical relativistic calculation we consider trajectories with vanishing kinetic momentum in polarization direction at the time of ionization and neglect I_p in the energy conservation condition. This shows that the effect of the ionization potential I_p on the cutoff energy is negligible at high laser intensities, i.e., the tunneling part of the electron dynamics has only little influence on the final energy of the ionized electron at high U_p.

The cutoff energy is maximal at the angle $\theta_{\max}$ determined by the condition

$$\left.\frac{\partial \varepsilon^F}{\partial \theta}\right|_{\theta=\theta_{\max}} = 0. \tag{36}$$

Figure 8 displays the dependence of the maximal cutoff energy on the laser intensity. Laser magnetic field and relativistic mass shift effects together increase the cutoff energy. Further, it can be seen that the calculations with leading nondipole and relativistic corrections are correct in the one-tenth of a percent area up to electron ponderomotive energies of U_p=300 a.u.

III. HIGH HARMONIC GENERATION

A. HHG based on the Klein-Gordon equation

HHG in the nonrelativistic domain is employed with success as a source for xuv radiation [44]. Shorter wavelength coherent radiation sources are required for different applications. Thus an increase of the HHG frequency becomes very desirable. The straightforward way to achieve it is to use a more intense driving laser field. It is then necessary to use relativistic regimes of HHG which we consider in this section.

Our treatment of HHG in the relativistic regime is based on the SFA. We proceed from the electron wave function as a solution of the Klein-Gordon equation in the form of Eq. (12), apply the SFA, replacing the exact Green function with the Volkov one $G(x,x') \to G^V(x,x')$, and calculate perturbatively the probability amplitude of harmonic photon emission, the electron interaction Hamiltonian with the harmonic field $V_H(x)$ being the perturbation Hamiltonian. This way, the HHG amplitude in the relativistic regime based on the Klein-Gordon equation is derived as follows [38]:

$$M_{\omega_H} = -i \int d^4x' \int d^4x'' [\Phi(x')^* V_H(x') \times G^V(x',x'') V_{AI}(x'') \Phi(x'')], \tag{37}$$

where ω_H is the harmonic frequency,

$$V_H(x) = 2\langle 1_H | \mathbf{A}_H(x)/c \cdot [\mathbf{p} + \mathbf{A}(\eta)/c] | 0_H \rangle,$$

$$\mathbf{A}_H(x) = c\sqrt{2\pi/\omega_H}\hat{\mathbf{e}}_H^* b^\dagger \exp(i\omega_H t - i\mathbf{k}_H \mathbf{r})$$

the vector potential of the harmonic field in the second quantization, with the polarization unit vector $\hat{\mathbf{e}}_H$ and the harmonic photon creation operator $b^\dagger$; $|l_H>$ are the states of the harmonic field with the number of photons l (l=0,1). Further, we apply the integration variable transformation $(ct',\mathbf{x}') \to (\eta',\mathbf{x}')$, $(ct'',\mathbf{x}'') \to (\eta'',\mathbf{x}'')$ with $\eta' = k^\mu x'_\mu$ and $\eta'' = k^\mu x''_\mu$. After assuming that the laser wavelength is much larger than the spatial extension of the wave packet of the ionized electron, we receive the emission rate for HHG,

$$M_{\omega_H} = \int_{-\infty}^{\infty} d\eta' \int_{-\infty}^{\eta'} d\eta'' \int d^3\mathbf{q}\, m^H(\mathbf{q},\eta',\eta'') \times \exp\{-i[S(\mathbf{q},\eta',\eta'') + (\omega_H/\omega)\eta']\}, \tag{38}$$

where $m^H(\mathbf{q},\eta',\eta'')$ is the HHG matrix element for emission in the laser propagation direction, the polarization of the emitted photon is chosen along the driving laser field,

$$m^H(\mathbf{p},\eta',\eta'') = -\sqrt{\frac{2\pi}{\omega_H}} \frac{c^2(p_x + A(\eta')/c)}{(2\pi)^{3/2}\varepsilon_{\mathbf{p}}\omega^2} \times \left\langle 0 \left| \mathbf{p} + \frac{\mathbf{A}(\eta')}{c} - \frac{\mathbf{k}}{\omega}(\varepsilon_{\mathbf{p}} + I_p - c^2) \right\rangle \right. \times \left\langle \mathbf{p} + \frac{\mathbf{A}(\eta'')}{c} - \frac{\mathbf{k}}{\omega}(\varepsilon_{\mathbf{p}} + I_p - c^2) \left| V \right| 0 \right\rangle. \tag{39}$$

Taking into account the periodicity of the HHG process in a long laser pulse, i.e., periodicity of the function $\int_{-\infty}^{\eta'} d\eta'' \int d^3\mathbf{q}\, m^H(\mathbf{q},\eta'\eta'') \exp[-iS(\mathbf{q},\eta',\eta'')]$ on the variable η', the HHG amplitude can be represented as

$$M_{\omega_H} = \sum_n \delta(n\omega - \omega_H)\omega \times \int_{-\pi}^{\pi} d\eta' \int_{-\infty}^{\eta'} d\eta'' \int d^3\mathbf{q}\, m^H(\mathbf{q}, \eta', \eta'') \times \exp\{-i[S(\mathbf{q}, \eta', \eta'') + n\eta']\}. \quad (40)$$

The probability of harmonic photon emission per unit time is given by

$$dw_{\omega_H} = \frac{|M_{\omega_H}|^2}{\mathcal{T}} d^3k_H, \quad (41)$$

with the interaction time $\mathcal{T}$. Then the differential rate of nth order HHG is

$$\frac{dw_n}{d\Omega} = n\omega \frac{\omega^2}{c^3} |M_n|^2, \quad (42)$$

where

$$M_n = \int_{-\pi}^{\pi} d\eta' \int_{-\infty}^{\eta'} d\eta'' \int d^3\mathbf{q}\, \tilde{m}^H(\mathbf{q}, \eta', \eta'') \times \exp\{-i[S(\mathbf{q}, \eta', \eta'') + n\eta']\}, \quad (43)$$

with

$$\tilde{m}^H(\mathbf{p}, \eta', \eta'') = -\frac{c^2[p_x + A(\eta')/c]}{(2\pi)^{3/2}\varepsilon_{\mathbf{p}}\omega^2} \times \left\langle 0|\mathbf{p} + \frac{\mathbf{A}(\eta')}{c} - \frac{\mathbf{k}}{\omega}(\varepsilon_{\mathbf{p}} + I_p - c^2) \right\rangle \times \left\langle \mathbf{p} + \frac{\mathbf{A}(\eta'')}{c} - \frac{\mathbf{k}}{\omega}(\varepsilon_{\mathbf{p}} + I_p - c^2)|V|0 \right\rangle. \quad (44)$$

In the long wavelength regime $\omega \ll I_p \ll U_p$, the saddle-point method of integration is applicable. The saddle-point condition yields

$$\tilde{q}_x = -\frac{\int_{\tilde{\eta}''}^{\tilde{\eta}'} d\tilde{\eta} A(\tilde{\eta})/c}{\tilde{\eta}' - \tilde{\eta}''},$$

$$\tilde{q}_y = 0,$$

$$\tilde{q}_z = \frac{\tilde{q}_x^2 + q_m^2/2}{\sqrt{c^2 - q_m^2 - \tilde{q}_x^2}},$$

$$\tilde{\varepsilon}_{\tilde{\mathbf{q}}}(\tilde{\eta}') = n\omega + c^2 - I_p,$$

$$\tilde{\varepsilon}_{\tilde{\mathbf{q}}}(\tilde{\eta}'') = c^2 - I_p, \quad (45)$$

with the ionization and rescattering phases $\tilde{\eta}''$ and $\tilde{\eta}'$, respectively, and the drift momentum $\tilde{\mathbf{q}}$.

B. HHG spectra in the relativistic regime

Using the standard saddle-point method, the HHG emission spectrum can be calculated. HHG spectra in the moderately relativistic regime (up to laser intensities of 3.6×10^{17} W/cm^2, $\lambda = 800$ nm) have been calculated in [23,33,36], via the Schrödinger equation with leading nondipole corrections or in [38] via the Klein-Gordon equation. At higher laser intensities, HHG is significantly suppressed in the case of a sinusoidal laser pulse. Therefore, we will limit ourselves in this section to the discussion of relations between the different approximations only. Figure 9 shows the HHG spectrum in the moderately relativistic regime under consideration. We recognize the same features in the spectra as in the ATI case when comparing the relativistic calculations with the nonrelativistic one, or the calculation including leading nondipole corrections. We see that the model with both nondipole and relativistic mass shift corrections is well applicable for the considered moderately relativistic regime. Further, including the correction due to the relativistic mass shift improves the agreement with the relativistic calculations essentially. We may point out that for low harmonic energies up to the center of the plateau (energy less than $2U_p$), both approximations give a HHG yield very close to the one of the relativistic treatment. This is due to the smaller importance of the relativistic corrections for rather slow electrons which generate low harmonics.

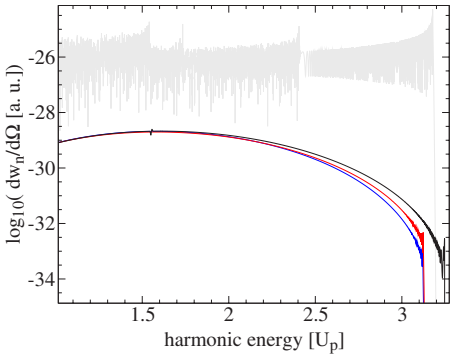

FIG. 9. (Color online) Harmonic emission rate in the laser propagation direction via $\log_{10}(dw_n/d\Omega)$ in Eq. (42) as a function of the harmonic energy: (gray, the first from top) within the dipole approximation, (black, second) with leading nondipole corrections, (red, third) Klein-Gordon equation, and (blue, fourth) with leading nondipole and relativistic mass shift corrections. The parameters of the driving laser field as well as of the atom are the same as in Fig. 2.

We conclude this section by investigating the laser intensity dependence of the cutoff energy for HHG in the moderately relativistic regime, see Fig. 10. The nondipole corrections account for the magnetic field induced drift and decrease the HHG probability as well as increase the cutoff energy [37]. Meanwhile, the relativistic mass shift correction counteracts the cutoff energy increase. In balance, the second effect is stronger and reduces the cutoff energies by 1% for the moderately relativistic regime. Similar to the case of ATI in this regime, the influence of the ionization potential on the cutoff energy can be neglected as the classical relativistic calculations show.

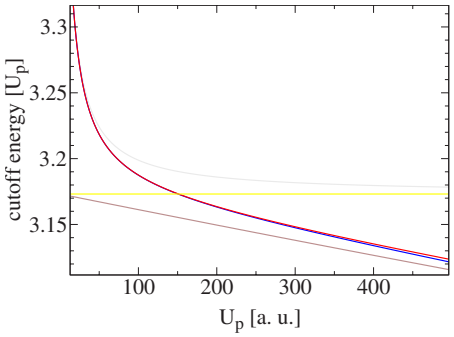

FIG. 10. (Color online) HHG cutoff energy scaled in multiples of U_p against the laser intensity represented by U_p: (gray, the first from top) within the dipole approximation, (yellow, second) classical nonrelativistic, (red, third) Klein-Gordon equation, (blue, fourth) with magnetic field corrections and the relativistic mass shift, (brown, fifth) classical relativistic. The parameters of the driving laser field as well as of the atom are the same as in Fig. 2.

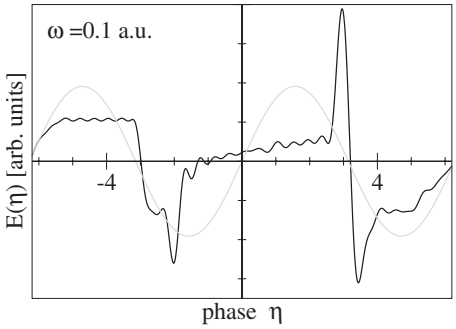

FIG. 11. Electric laser field $E(\eta)$ of the preliminary tailored pulse (black) compared with a sinusoidal pulse (gray) with the same average intensity.

IV. RESCATTERING IN THE TAILORED PULSES

A. The procedure for tailoring laser pulses

In the preceding sections we use a conventional sinusoidal laser field to ionize the atom and to drive HHG. Due to the laser magnetic field induced drift of the ionized electron, the probability of the electron rescattering is essentially suppressed compared with the nonrelativistic case. Is it possible to modify the laser pulse in such a way that it enables the ionized electron to rescatter with the ionic core more effectively in the relativistic regime, and thus, enables HHG in the hard x-ray domain?

To answer this question, it is instructive to analyze the ionized electron trajectories in the sinusoidal laser field. After the ionization, the electron is accelerated by the laser field, which alternated by deceleration due to the change of the laser field phase. In the deceleration phase, the electron loses almost all the energy acquired in the first phase. As a result, all of the energy the electron possesses at the recollision moment which is transferred into HHG is accumulated during the third and last acceleration phase (see corresponding figures in Secs. IV B and IV C). Hence, the first two acceleration-deceleration phases do not contribute to the energy gain of the electron, but what is more dramatic, they contribute to the induced relativistic drift. This instructs how to decrease the relativistic drift without significant change of the rescattering energy. The laser pulse should be tailored in such a way that its field strength decreases strongly after the phase of ionization and, has a short strong burst before recombination. The relativistic drift will be significantly smaller in such a tailored pulse because the time span during which the electron moves with relativistic velocity within is much shorter than in the sinusoidal laser pulse.

Now, we proceed to tailor the laser pulse with the aim of enhancing the rescattering probability without a decrease of the rescattering energy in a laser field of a certain average intensity. The procedure of the pulse tailoring is the following. We start with a trial laser pulse in a temporal form $E(t)$ which allows in a preliminary form the features outlined above. The pulse is expressed as a Fourier expansion

$$E(t) = \sum_{k=-K}^{K} c_k \exp(ik\omega_0 t), \tag{46}$$

with the angular ground frequency $\omega_0=0.1$ a.u., the Fourier coefficient $c_k^*=c_{-k}$ and the maximum number of employed harmonics K. In the next step, the Fourier coefficients are modified to maximize the rescattering probability at a certain cutoff energy for ATI/HHG. For maximizing the rescattering probability, we invoke the SFA along with the saddle-point method. The saddle-point conditions of Eq. (24) and the cutoff condition of Eq. (35) determine the ionization and the rescattering times at the cutoff energy $\tilde{\eta}, \tilde{\eta}, \tilde{\varepsilon}^F$. The imaginary part of the ionization time $\mathrm{Im}(\tilde{\eta})$ is connected with the ionization probability. At a fixed drift momentum $\tilde{\mathbf{q}}$, the larger the ionization probability is, the larger the rescattering probability. Thus, the imaginary part of the ionization time is a measure for the rescattering efficiency. We fix the cutoff energy $\tilde{\varepsilon}^F$ and minimize the imaginary part of the ionization time $\mathrm{Im}(\tilde{\eta})$ by varying the coefficients c_k of the pulse. The preliminary tailored pulse is displayed in Fig. 11. It consists of a peak which is responsible for the ionization of the electron, and two peaks shortly before and after the rescattering which induce most of the energy the electrons gain on their path. The first and the second peak are separated by approximately 500 attoseconds as whereas the second and third are separated by approximately 50 attoseconds. Further, we can identify several features of this tailored pulse which are important for the enhancement of the rescattering efficiency. First, the decay of the laser field after the time of ionization should be strong (the stronger the better). Thus, the electron receives only a short kick in the polarization direction by the laser field and has no opportunity to drift in the laser propagation direction. Second, the pulse responsible for the ionization should be followed by a time span (the longer the better) with a comparably weak laser field strength, where the ionized electron can propagate in the continuum with a nonrelativistic velocity (i.e., little drift), followed again by two oppositely directed huge peaks which induce most of the energy the electron gains on its path. Since these two peaks also have a short duration, the drift in the laser propagation direction is reduced. Further, the change of the laser field strength at the time of rescattering, i.e., between the two peaks, should be very strong (the stronger the better). The

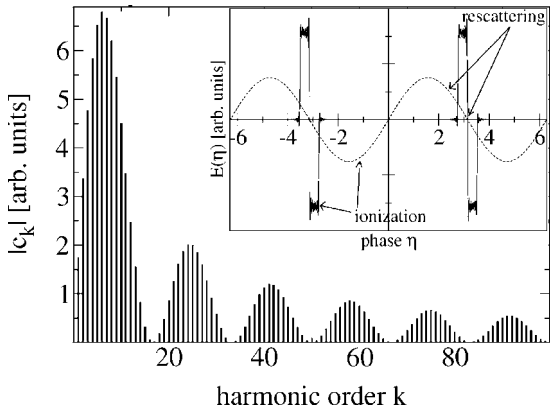

FIG. 12. The tailored pulse: the frequency spectrum of the tailored pulse $|c_k|$. The harmonics in the tailored pulse are phase locked; in the inset, the laser field $E(\eta)$ of the tailored pulse (black) is compared with a sinusoidal pulse (dashed) with the same average intensity and an angular frequency of $\omega=0.1$ a.u. The pulse duration of the APT is $\omega\tau=0.12\pi$.

property of the pulse that is most important and must be strictly fulfilled is the strong decay after ionization whereas the shape of the energy-supplying peaks is more or less arbitrary.

It is possible to find a pulse form that includes all the listed features and at the same time is rather simple to generate, as it has a smooth frequency and phase spectrum. This can be achieved by a pulse consisting of two oppositely directed rectangular peaks per laser period that are divided by a long field free region, compared to the width of the rectangular peaks. We use 100 harmonics of the ground frequency $\omega=0.1$ a.u. to reproduce and optimize this kind of a tailored pulse as shown in Fig. 12 via its frequency and phase spectrum. Actually, the tailored pulse represents in itself an attosecond pulse train (APT), with the pulses having a rectangularlike shape. In what follows, we compare results of ATI and HHG using our tailored pulse with a sinusoidal pulse at the same ground frequency.

B. ATI in the tailored laser pulse

We do a full-relativistic calculation of the photoelectron spectrum in the tailored pulse shown in Fig. 12 and compare it with the photoelectron spectrum in the sinusoidal laser field with the same average intensity. As a reference tool to indicate the impact of the relativistic drift, we calculate also the electron spectrum in a sinusoidal laser wave in the dipole approximation when there is no drift. We will see that the tailoring of the laser pulse allows rescattering in strong relativistic regimes.

First, we consider the moderately relativistic regime with a laser intensity of 1×10^{18} W/cm^2. For calculating the integral in Eq. (16), we use the saddle-point method that is justified in the case of an APT with a spectral content that is not very rich, $K\omega \ll I_p$. The spectra of the rescattered electrons are shown in Fig. 13. The tailored pulse delivers ATI rates that are about 10 orders of magnitude larger than those obtained with a conventional sinusoidal wave in the relativistic

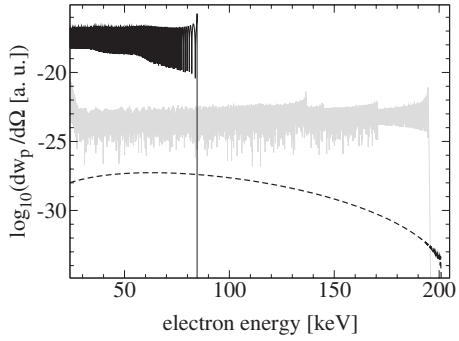

FIG. 13. Photoelectron spectrum via $\log_{10}(dw_{\mathbf{p}}/d\Omega)$ in Eq. (21), with final electron momentum in the direction with maximal cutoff for an atomic ion with ionization potential $I_p=18$ a.u. in a laser field with average intensity of 1×10^{18} W/cm^2 and angular frequency $\omega=0.1$ a.u.: (gray) within the dipole approximation and a sinusoidal wave, (dashed) Klein-Gordon equation and a sinusoidal wave, (black) Klein-Gordon equation and the tailored pulse.

treatment. The nonrelativistic calculations are not accurate for the considered parameter regime but are used as a reference for the ideal ionization-rescattering scenario. The features of the electron spectrum in the tailored pulse resemble those of the nonrelativistic spectrum. In particular we have almost a flat but oscillating plateau instead of a bending and a nonoscillating one. The fluctuation of the spectrum results from the interference of the two trajectories of shortest duration. Contributions from trajectories with multiple return to the core that are possible in the nonrelativistic case are very unlikely for the tailored pulse. That is why there is no multiplateau structure. The cutoff of the spectrum is at about 70 keV which is less than in the sinusoidal wave. In the tailored pulse we obtain rescattering rates that are even higher than the result based on the dipole approximation; namely, the enhancement reaches approximately six orders of magnitude.

Figure 14(a) displays the trajectory of the ionized electron due to the tailored pulse and a sinusoidal wave, respectively. The excursion of the ionized electron in the polarization and propagation direction for a tailored pulse is smaller, though the driving laser intensity is the same as for a conventional sinusoidal wave. Moreover, we see that the emission angle of the electron in the tailored pulse at the ionization moment is much more directed along the laser polarization direction than for the conventional sinusoidal wave. This is an indicator of the decreased electron velocity in the laser propagation direction at the ionization moment, and consequently, an indicator of the increased ionization rate and the higher rescattering efficiency. The initial momentum in the laser propagation direction for the rescattering electron in the tailored pulse is −0.26 a.u. while in the sinusoidal wave it is −4.7 a.u. The second observation is that the laser electric field strength at the ionization phase of −11.5 a.u. is stronger compared with −5.2 a.u. in the sinusoidal wave. This is the reason for the increase of the ATI rate in the tailored pulse compared with the result in the dipole approximation for a sinusoidal wave.

In Fig. 14(b) we display the energy of the ionized cutoff electron in its trajectory. While in the sinusoidal wave the

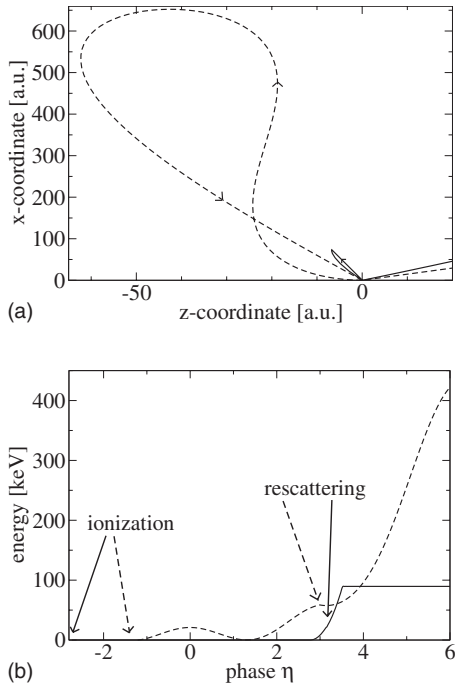

FIG. 14. (a) Trajectory and (b) kinetic energy of an ATI cutoff electron in the tailored wave (solid line) and in a sinusoidal wave (dashed line) with an average laser intensity of 1×10^{18} W/cm^2. (x and z are the polarization and propagation direction of the laser field, respectively.) The electron is ionized at a phase of -1.31 in the sinusoidal wave and rescatters at a phase of 3.00. In the tailored wave the electron is ionized at a phase of -2.79 and rescatters at a phase of 3.14.

electron energy oscillates during the excursion, in the tailored pulse the electron gains most of its energy shortly before and after rescattering. Its energy at the time of rescattering is approximately a third of the final energy.

High-energy ATI spectra in the full relativistic regime for a laser intensity of 1×10^{19} W/cm^2 are shown in Fig. 15. The result is qualitatively the same as in the moderately relativistic regime but quantitatively more pronounced. Whereas

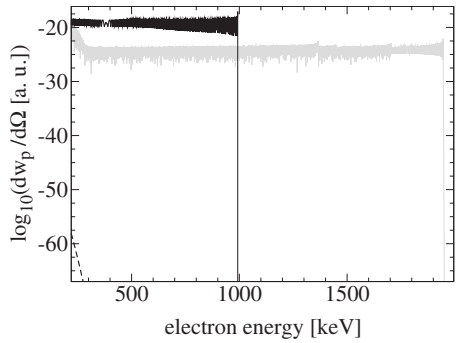

FIG. 15. Photoelectron spectrum via $\log_{10}(dw_{\mathbf{p}}/d\Omega)$ in Eq. (21), with final electron momentum in the direction with maximal cutoff energy applying a laser with an intensity of 1×10^{19} W/cm^2 and an ionization potential $I_p=38$ a.u.: (gray) within the dipole approximation and a sinusoidal pulse, (dashed) Klein-Gordon equation and a sinusoidal pulse, (black) Klein-Gordon equation and the tailored pulse.

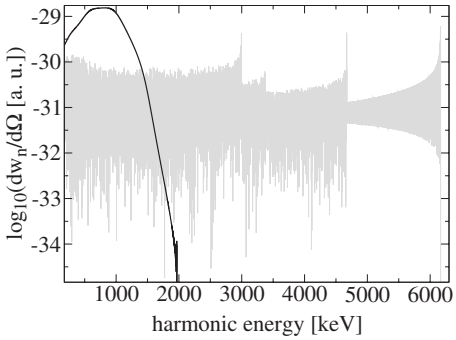

FIG. 16. Harmonic emission rate in the laser propagation direction via $\log_{10}(dw_n/d\Omega)$ in Eq. (42) as a function of the harmonic energy with a laser intensity of 1×10^{20} W/cm^2: (gray) within the dipole approximation and a sinusoidal wave, (black) Klein-Gordon equation and the tailored pulse. The spectrum with Klein-Gordon equation and a sinusoidal wave is many orders of magnitude smaller and is not displayed. The ionization potential is adapted to the threshold of the barrier-suppression model, $I_p=82$ a.u.

the results based on the relativistic treatment of a sinusoidal wave are totally negligible, the rates from the tailored pulse are still about five orders of magnitude larger than the rates when using a sinusoidal wave within the dipole approximation. Final electron energies of about 1 MeV become possible with the applied parameters.

C. HHG in the tailored laser pulse

As the tailored laser pulses can increase the energy of the rescattered electron, one can employ it to achieve HHG in a short-wavelength domain. The optimization of the tailored pulse in the case of HHG is carried out by the use of the saddle-point conditions of Eqs. (45) along with the cutoff condition

$$\frac{d\tilde{\varepsilon}_{\tilde{\mathbf{q}}}(\eta')}{d\eta''}=0, \tag{47}$$

for the ionization, recombination phases $\tilde{\eta}'', \tilde{\eta}'$, and the harmonic number of the emitted photon $\tilde{n}$. It is not surprising that the optimized pulse for ATI presented in Sec. IV A in fact serves as the optimized one for HHG, because in both cases the probability of rescattering is optimized for a fixed energy of the electron at the moment of revisiting the ionic core. Hence, we use the APT shown in Fig. 12 to calculate HHG in relativistic regimes. Then, the HHG scenario is as follows. The electron is ionized at the end of the attosecond pulse, propagates during the field free region, acquires energy during the following attosecond pulse, and recombines after it with emission of high-harmonic radiation. In [34] we have presented HHG spectra obtained via the tailored pulses in the moderate relativistic regime. Here we continue the HHG investigation in the strong relativistic regime, applying a laser intensity of 1×10^{20} W/cm^2. In Fig. 16 the HHG spectra in the strongly relativistic regime are displayed. The spectrum generated by the tailored pulse in the laser propagation direction is compared with that of a sinusoidal laser field in the nonrelativistic treatment. The HHG rate when

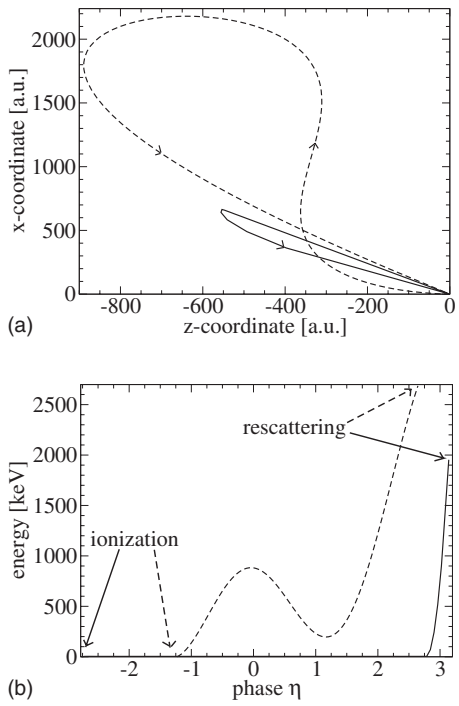

FIG. 17. (a) Trajectory and (b) kinetic energy of the electron producing HHG of the cutoff energy in the tailored pulse (solid) and in a sinusoidal wave (dashed), each with an average intensity of 1×10^{20} W/cm^2. x and z are the polarization and propagation direction of the laser field, respectively. The electron is ionized at a phase of -1.24 in the sinus wave and recombines at a phase of 2.64. In the tailored wave the electron is ionized at a phase of -2.78 and recombines at a phase of 3.14.

using the tailored pulse is comparable or even higher than the rate with the sinusoidal wave in the ideal case of the dipole approximation up to energies of the emitted radiation of 1.5 MeV. The spectrum when using a sinusoidal wave calculated with the correct Klein-Gordon equation is many orders of magnitude (at least 30) smaller and is not displayed.

In Fig. 17(a) the trajectories of the electron delivering the HHG cutoff energy in the tailored pulse are compared with that in a sinusoidal pulse. It is visible that the electron in the tailored pulse can start with a much smaller velocity against the laser propagation direction and nevertheless recombines with the atomic core. Further the trajectory in the tailored pulse is much smaller than in the sinusoidal wave, even though both laser intensities are equal.

In Fig. 17(b) the energy of the HHG cutoff electron in its trajectory in the tailored pulse and in a sinusoidal wave with the same intensity is displayed. One can see that the electron in the tailored pulse gains most of its energy only shortly before recombination and thus moves only for a short time with a strongly relativistic velocity which results in an essential reduction of the relativistic drift compared to the case of a conventional sinusoidal driving laser field.

D. Influence of the shape of the tailored pulse on the rescattering

The APT is chacterized by four parameters: the harmonic content, i.e., the amount of harmonics that build up the attosecond pulse, the duration of the pulse in the train, the time delay between the pulses, equivalent to the ground angular frequency and the maximal field strength of the pulse that is connected with the laser intensity. In this section we investigate the dependence of the HHG yield on the parameters: (1) harmonic content of the APT, at a fixed duration of the pulses in the train, a fixed ground angular frequency and a fixed intensity, (2) duration of the pulse in the train at a fixed ground frequency of the APT, a fixed harmonic content, and a fixed average intensity of the APT; (3) time delay between the pulses in the train at a fixed duration of each pulse in the train, a fixed harmonic content of the APT, and a fixed amplitude of the pulse.

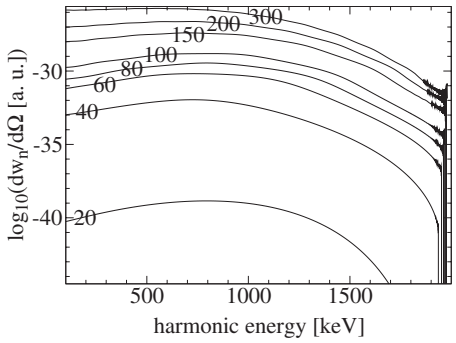

FIG. 18. Harmonic emission rate via $\log_{10}(dw_n/d\Omega)$ in Eq. (42) as a function of the emitted photon energy in a laser intensity of 1×10^{20} W/cm^2 and ground angular frequency of $\omega=0.1$ a.u. using tailored pulses which consist of 20, 40, 60, 80, 100, 120, 150, 200, and 300 harmonics of the ground frequency. The ionization potential is $I_p=82$ a.u.

Let us investigate how important the different harmonics are that build up the tailored pulse. The ground frequency of the APT which determines the duration between pulses in the train is maintained constant. We also fix the duration of the pulses in the train. Consequently, the characteristic frequency of the spectrum, which determines the pulse duration, is also fixed. From Fig. 12(b) one can see that the characteristic frequency in the applied case is 20ω. We change the number of the humps in the spectrum of the driving APT field, keeping the shape of the humps as in Fig. 12(b). The increase of the number of harmonics in this way actually presumes that the pulse shape approaches more and more the rectangular form. The result of the calculation of the spectra for the HHG process when using the tailored pulse with a different maximum number of applied harmonics are shown in Fig. 18.

The more rectangularlike the pulse shape is (i.e., the larger number of applied harmonics at a fixed pulse duration and a fixed APT ground frequency), the larger the HHG yield and the HHG cutoff energy. While the increase in the cutoff energy is very small, the increase in the HHG rate is tremendous. In fact, an increase in the harmonic content from 20 up to 40 increases the energy gain only by 13%, whereas the HHG yield becomes more than seven orders of magnitude larger. Hence, the HHG rate is very sensible to the fine structure of the APT which is tuned by the harmonic content of the tailored pulse. Meanwhile, the electron energy gain is mainly determined by the duration of the pulse. Whereas the first 20 harmonics reproduce the general shape of the APT,

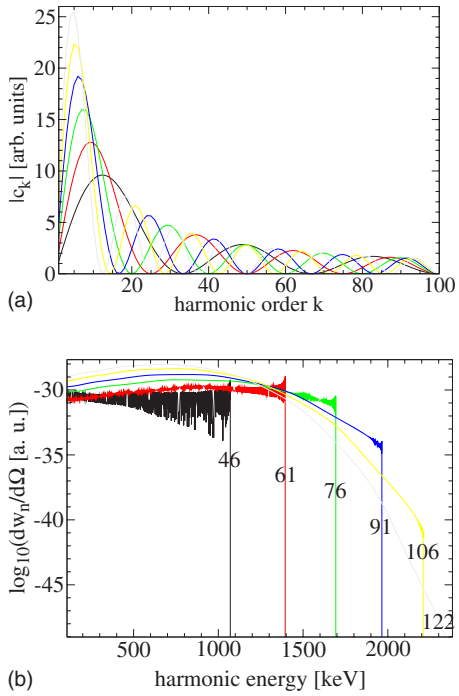

FIG. 19. (Color online) The dependence of the HHG rate on the duration of the pulse in APT: (a) frequency spectrum of APT's with different pulse length in the train, $(2\pi/\omega)(k/100)$, where k is the amount of humps. (b) The resulting harmonic emission rate via $\log_{10}(dw_n/d\Omega)$ in Eq. (42) as a function of the emitted photon energy using these tailored pulses. The pulse duration in the train (in attoseconds) is given in the figure corresponding to $k=3$ up to $k=8$. The laser average intensity is 1×10^{20} W/cm^2. The ionization potential is adapted to the threshold of the barrier-suppression model.

particularly the pulse duration in the train, one can say that the small harmonics are responsible for the energy the electron gains from the pulse while the higher harmonics assure that the electron recombines effectively with the atomic core. Further, our calculations show that the tailored pulse is sufficiently built up by 100 harmonics. The application of even more harmonics has only a small effect on the emission rate.

The tendency that enrichment of the harmonic content of the APT results in an increase of the rescattering probability and an energy gain of the electron is intuitively understandable. The APT with a rich harmonic content resembles more to a train of rectangular pulses. Then there are no small field oscillations inducing parasitic oscillations of the electron energy that consequently cause additional relativistic drift. Further, the laser field descent after ionization is more sharp and makes it impossible for the electron to acquire a relativistic velocity and, therefore, to drift.

Now, we turn to the investigation of the dependence of the HHG rate on the duration of the pulse in the APT. In Fig. 19 we compare HHG spectra generated by an APT with the tailored shape and a ground frequency of 0.1 a.u. for different durations of the pulse in the train. The harmonic content of the APT is fixed at $K=100$. The amount of humps in the frequency spectrum of the pulses indicates the duration of the pulse. The average laser intensity is fixed at 1×10^{20} W/cm^2, and the ionization potential is chosen so that

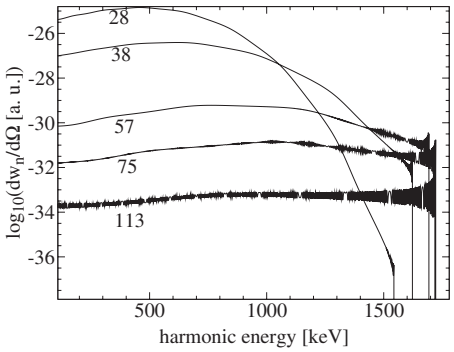

FIG. 20. Harmonic emission rate via $\log_{10}(dw_n/d\Omega)$ in Eq. (42), as a function of the harmonic energy using tailored APTs consisting of pulses with a temporal width of π a.u. and a time delay between the pulses of 28, 38, 57, 75, and 113 a.u., respectively. The maximum laser electric field strength is fixed at a value of 140 a.u. The ionization potential is $I_p=82$ a.u.

it is in the tunneling regime but close to the border of over-the-barrier ionization.

One can see that the harmonic cutoff scales approximately linear with the width of the pulses due to the increase in the duration of the accelerating phase. The HHG yield at the cutoff decreases significantly with an increased pulse width. In the case of a shorter pulse duration, the ionization of the rescattering electron occurs at a moment closer to the end of the pulse and consequently, the momentum in the laser propagation direction, necessary for rescattering has a lower value (see also Sec. IV E below). The spectra resulting from broader pulses are less oscillating and more strongly bent, indicating the stronger relativistic character of the process. By comparison to tailored pulses with different duration but with adapted intensities that deliver the same fixed cutoff, one can see that for lower emission energies larger widths are favored whereas at the cutoff, shorter widths are better suited.

Finally, we investigate the dependence of the HHG yield on the time delay between the pulses in the APT. In Fig. 20 we compare the HHG spectra generated by an APT with the tailored shape (with a number of harmonic content of $K=100$) and a pulse duration of π a.u. for different ground frequencies of the APT, i.e., for different free time spans between the pulses. The maximum laser electric field strength of the pulse is fixed at a value of 140 a.u. First, one can see that the cutoff energy is decreasing only weakly with a decreased free time span between the pulses in the train. This can be explained by the fact that due to a shorter field free time span, the electron has less time to propagate in the continuum and therefore can acquire less energy from the laser on its way back to the atomic core. Further, the relativistic signature of the process, displayed by an increase in the bend of the spectrum and a decrease in the interference pattern, increases with decreasing free time span. This occurs as the relative time span where the ionized electron moves with a relativistic momentum compared to the one where the electron moves nonrelativistically becomes larger (see also Sec. IV E). The HHG yield at the cutoff increases with an increased free time span from 28 a.u. up to 57 a.u., but then decreases slightly when the free time span changes from

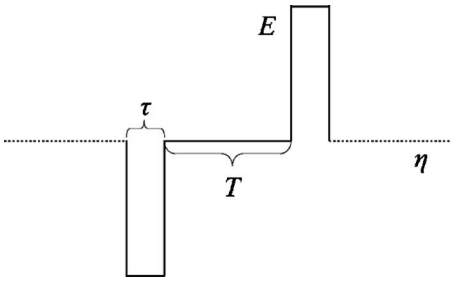

FIG. 21. A model APT consisting of one cycle rectangular pulses that mimic the tailored APT of Fig. 12 for the purpose of an analytical analysis of the electron dynamics.

57 a.u. up to 113 a.u. This is due to the counteraction of two tendencies: the relativistic signatures in the electron dynamics and the spreading of the ionized electron wave packet. Finally, to obtain a high emission rate for high energies in the MeV domain, an intermediate time delay of about a femtosecond (57 a.u.), i.e., an angular frequency of approximately 0.1 a.u., is best suited. Then the relativistic effects, the spreading and the energy gain effect as described above are balanced.

E. Dynamics of the electron in a rectangular APT

For a better insight into the rescattering process in the strong field of the tailored APT, let us consider analytically the problem of electron ionization-excursion-rescattering in a model APT. The latter consists of a sequence of one-cycle rectangular oscillations of a duration τ separated by a field free region of duration T (see Fig. 21). We analyze electron trajectories in this field via the classical equations of motion and calculate the energy gain of the electron at the rescattering moment.

The vector potential of the laser field (see Fig. 21) can be expressed as

$$\mathbf{a}(\eta) = \hat{\mathbf{x}} a_0 \begin{cases} -\eta, & 0 \leqslant \eta \leqslant \eta_1, \\ -\eta_1, & \eta_1 \leqslant \eta \leqslant \eta_1 + 2\pi, \\ \eta - 2\eta_1 - 2\pi, & \eta \geqslant \eta_1 + 2\pi, \end{cases} \tag{48}$$

where $\mathbf{a}(\eta)=\mathbf{A}(\eta)/c^2$, $a_0=A_0/c^2$, $\eta=\omega(t-z/c)$, the x and z axes are aligned in the laser polarization and propagation direction, respectively. The ionization takes place at $\eta_0=0$, the field free region spans from η_1 up to $\eta_1+2\pi$.

The electron is ionized with zero transversal momentum but the longitudinal momentum is not zero allowing the electron to revisit the atomic core. Consequently, we use Eqs. (30) with $p_x=0$. The probability of the electron to tunnel out of the atom with nonzero initial momentum p_{z0} is exponentially decreasing with increasing p_{z0} [23]. Therefore, the suppression of the relativistic drift can be recognized by a decrease in the p_{z0} value, which is necessary for rescattering.

The electron coordinates in the considered case are determined as follows (see, e.g., Ref. [43]):

$$x = x_0 + \frac{c^2}{\omega}\int_{\eta_0}^{\eta} \frac{d\eta'}{\Lambda}[a(\eta) - a(\eta_0)],$$

$$z = z_0 + \frac{c}{\omega}\int_{\eta_0}^{\eta} \frac{d\eta'}{\Lambda}\left(p_{z0} + c^2\frac{[a(\eta_0) - a(\eta)]^2}{2\Lambda}\right). \tag{49}$$

When using the explicit form of the vector potential of Eq. (48), the electron coordinates read

$$x - x_0 = \frac{a_0}{\omega}\frac{c^2}{\Lambda}\left(\eta_1^2 + \eta_1 2\pi - \frac{(\eta_2 - \eta_1)^2}{2}\right),$$

$$z - z_0 = \frac{c}{\omega}\frac{p_{z0}(\eta_1 + \eta_2 + 2\pi)}{\Lambda} + \frac{a_0^2}{\omega}\frac{c^3}{2\Lambda^2}\left(\frac{2\eta_1^3}{3} + 2\pi\eta_1^2 + \frac{(\eta_2 - \eta_1)^3}{3}\right), \tag{50}$$

where η_2 determines the recollision phase $\eta_r=\eta_2+\eta_1+2\pi$, where $x=x_0$ and $z=z_0$. The first of these conditions gives

$$\eta_2 - \eta_1 = \sqrt{2(\eta_1^2 + 2\pi\eta_1)}, \tag{51}$$

while from the second one p_{z0} is determined,

$$p_{z0} = -\frac{c^2}{2\Lambda}a_0^2\frac{\left(\frac{2\eta_1^3}{3} + 2\pi\eta_1^2 + \frac{(\eta_2 - \eta_1)^3}{3}\right)}{(\eta_1 + \eta_2 + 2\pi)}. \tag{52}$$

According to the definition,

$$\eta_1, \eta_2, |\eta_2 - \eta_1| \leqslant \omega\tau. \tag{53}$$

Then at $\omega\tau \ll 2\pi$, it is

$$\eta_2 - \eta_1 \approx \sqrt{4\pi\eta_1}. \tag{54}$$

From the latter condition one can deduce the maximal value of η_1 for the rescattering electron,

$$\eta_1^{\max} = \frac{\pi\tau^2}{T^2}. \tag{55}$$

Thus, for revisiting the ionic core the ionized electron should have the initial longitudinal momentum in leading order

$$p_{z0}^{(\mathrm{APT})} = -c\frac{2\pi^2}{3}a_0^2\frac{\tau^3}{T^3} = -\frac{\pi}{3}\frac{\bar{I}}{c^2}\tau^2. \tag{56}$$

The gain of energy of the rescattering electron in the APT can be calculated from Eq. (30) which yields

$$\Delta\varepsilon^{(\mathrm{APT})} = 2\pi^2c^2a_0^2\frac{\tau^2}{T^2} = \frac{\pi\bar{I}\tau T}{c}, \tag{57}$$

where $\bar{I}=cE_0^2 2\tau/4\pi T$ is the average laser intensity. Let us compare the energy gain and the initial longitudinal momentum of the rescattering electron (which is the measure of the significance of the relativistic drift) for two cases of an APT and a sinusoidal laser wave at the same average laser pulse intensity. In the sinusoidal laser wave it is known that

$$\Delta\varepsilon^{(L)} \approx \frac{3c^2a_0^2}{4} \approx \frac{3IT^2}{2\pi c},$$

$$p_{z0}^{(L)} \approx -c\frac{a_0^2}{4} \approx -\frac{IT^2}{2\pi c^2}, \tag{58}$$

with the laser intensity $I=cE_0^2/8\pi$. The comparison shows

$$\frac{\Delta\varepsilon^{(\mathrm{APT})}}{\Delta\varepsilon^{(L)}} \approx \frac{2\pi^2}{3}\frac{\tau}{T},$$

$$\frac{p_{z0}^{(\mathrm{APT})}}{p_{z0}^{(L)}} \approx \frac{2\pi^2}{3}\left(\frac{\tau}{T}\right)^2, \tag{59}$$

which means that choosing a rather small pulse duration (τ) compared with the period (T) will decrease significantly the necessary initial momentum (p_{z0}), suppressing the relativistic drift, while the decrease in the cutoff energy will not be significant.

F. The stability of the HHG process against random variations of the shape of the tailored pulse

In this section we answer the question of how robust the effect of enhancing the HHG yield via tailored pulses is. We represent results of the investigation of the stability of the HHG process vs a random variation of the shape of the tailored pulse. We employ APTs whose spectral components are randomly varied from the optimal values. We can say that a random variation of the absolute values of the spectral components of the pulse of about 5% (see Fig. 22) or of the phases of the spectral components of about $\pi/100$ (see Fig. 23) changes the emission rate near the cutoff by about one order of magnitude at the most.

G. Generation of tailored pulses

From the discussion presented in the preceding sections we have derived requirements for realizing HHG in the relativistic regime via tailored pulses. The tailored pulses are required to have an APT shape with a ground frequency of 0.1 a.u. (corresponding to a field period of about 1 fs), a pulse duration in the train of about 50 attoseconds and an average intensity of 1×10^{19} W/cm^2. The optimal number of harmonic content is 40–60. These are the optimal parameters of the tailored laser pulse for HHG in the relativistic regime.

The main difficulty in experimental realization of this kind of pulse is the combination of two extreme properties: a pulse train of attosecond duration and high intensity. A few laboratories are now able to produce attosecond pulse trains [45] which are based on HHG in gases with further filtering of the harmonics and reshaping the pulse. Unfortunately, the method of APT via HHG in gases has no potential for higher intensities of xuv radiation. This is because the efficiency of this mechanism is small, not exceeding 10^{-5}, and the driving laser intensity is restricted by the ionization cap. Therefore, one must look for alternative methods for strong attosecond pulse generation. Laser-plasma interactions seem to be the most suitable nonlinear phenomena which could be employed for attosecond pulse generation at high intensities. First of all, where high intensities are concerned, then plasma is the ideal medium as the ionization restriction is automatically removed. Second, at relativistically high laser intensities new kinds of nonlinearities of the plasma arise. On the one hand, the free electron dynamics becomes nonlinear at $a_0>1$, on the other hand in overdense plasma (especially at the interface between vacuum and plasma) high gradients of the field and of the particle density emerge in a strong laser field which are extremely benevolent properties for nonlinear transformation of the incoming strong laser field. Apart from these general arguments in favor of the plasma as a medium for the optical field transformations into an APT, two recently uncovered regimes of the strong laser field plasma interactions give us additional hope that our proposed requirements for APTs are realizable.

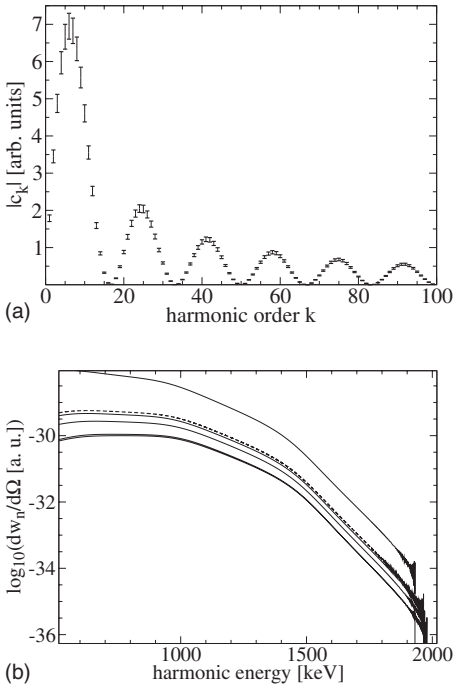

FIG. 22. (a) The variation of the absolute value of the spectral components of the APT with a pulse duration in the train of $0.12\pi/\omega$, and $\omega=0.1$ a.u. is displayed. The random variation from the optimal values is within 5%. (b) The resulting emission rate via $\log_{10}(dw_n/d\Omega)$ in Eq. (42) as a function of the harmonic energy using five different randomly varied tailored pulses with an intensity of 1×10^{20} W/cm^2. The dashed curve corresponds to the unperturbated tailored pulse. The ionization potential is $I_p=82$ a.u. The APT contains 100 harmonics.

The first regime is the sliding-mirror regime of a relativistically strong laser beam interacting with a thin plasma layer [47]. This regime is realized when the plasma is so dense that even in the strong laser field, the electron displacement along the laser propagation direction is negligible. This is realized under the condition $\epsilon_p \approx a_0$, where $\epsilon_p \equiv \pi(n/n_{cr})(L/\lambda)$, n is the plasma density, $n_{cr}=m\omega/4\pi e^2$ is the plasma critical density, L is the plasma layer length, ω and λ are the laser frequency and the wavelength. One can see from this condition that high densities, thin layers, and strong laser fields are required for this regime to operate. Although, harmonics are generated in the reflected as well as in the transmitted light, in the latter case APT can be produced without additional harmonic filtering as the generated

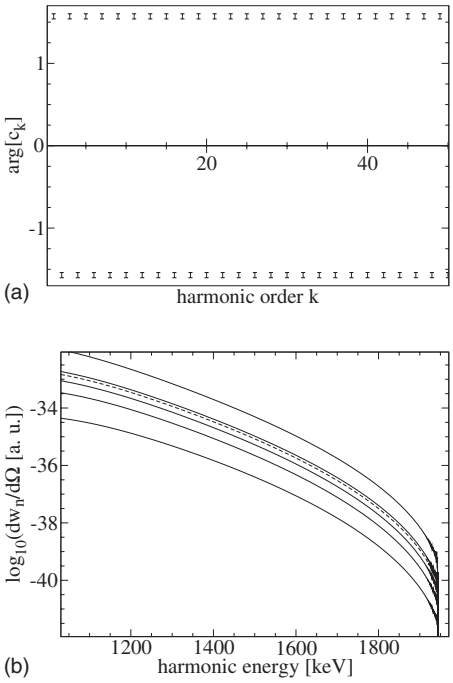

FIG. 23. (a) The variation of the phase of the spectral components of the APT with a pulse duration in the train of $0.12\pi/\omega$, and $\omega=0.1$ a.u. is displayed. The variation from the optimal value is within $\pi/100$. (b) The resulting emission rate via $\log_{10}(dw_n/d\Omega)$ in Eq. (42) as a function of the harmonic energy when using five randomly varied tailored pulses with an intensity of 1×10^{20} W/cm^2. The dashed curve corresponds to the unperturbated tailored pulse. The APT contains 50 harmonics.

harmonics are well phase locked. Since spectral filtering can be avoided, the energetic efficiency of APT generation enhances, as particle-in-cell (PIC) simulations of [47] show, reaching a few percent. The characteristic frequency of the HHG spectrum in this regime is $\omega_{cr}=a_0\omega$ which determines the fastest time scale of an APT (i.e., the pulse duration in the train). Then, a laser field with $a_0\approx20$ will correspond to our requirements.

The second regime, which can be employed to realize our proposed tailored laser pulses, is the λ^3 regime of laser beam reflections from overdense plasma surfaces [46]. Here the plasma nonlinearity is mainly based on high gradients of the field and of the particle density at the plasma surface. PIC simulations have shown that in this regime isolated attosecond pulses can be generated with a very high efficiency of about 10%. Then one can think of the generation of half-cycle strong pulses and combine them in the train, this way realizing the requirements of our tailored pulses. Nevertheless, more investigation is necessary to determine whether the requirements of the harmonic content, the duration and other parameters can be met in these regimes. Moreover, these regimes still must be confirmed experimentally. Taking into account the very rapid development of the strong field laser-plasma interaction field and the fact that proposals for stronger laser pulses are at this stage [48], one can be optimistic about the outcome.

V. CONCLUSION

By a fully relativistic treatment we have investigated features of the energy and angular distribution of electrons in ATI and of HHG spectra in relativistic regimes. A comparison with the approximate theory for the weakly relativistic regime is drawn, and the limitations of the latter are pointed out.

To enhance the yield of high-energy electrons in ATI and high-energy photons in HHG in the relativistic regime, a method is proposed based on the application of specially tailored laser pulses. Specially tailored laser pulses in the form of an APT allow the suppression of the relativistic drift of the ionized electron and ionization rescattering in the relativistic regime. We have investigated in detail ATI and HHG properties in the tailored pulses. In particular, the dependence of the HHG yield on the pulse length in an APT, on the time delay between the pulses in an APT and on the harmonic content on the APT is studied and explained by means of a simple analytical analysis of the electron dynamics in the APT consisting of rectangular pulses.

As a result of the investigation, we can give the optimal parameters for the tailored pulses. The tailored pulses with a ground frequency of 0.1 a.u., pulse duration in the train of 50 attoseconds, with a harmonic content of 40–60, and with an average intensity of 10^{19} W/cm^2 are the desired pulse shapes for the optimized HHG/ATI. This way, HHG in the hard x-ray domain and the initiation of nuclear reactions with single ions will become feasible.

ACKNOWLEDGMENT

Funding by Deutsche Forschungsgemeinschaft via KE-721-1 is acknowledged.

[1] P. Agostini, F. Fabre, G. Mainfray, G. Petite, and N. K. Rahman, Phys. Rev. Lett. **42**, 1127 (1979); P. H. Bucksbaum, M. Bashkansky, R. R. Freeman, T. J. McIlrath, and L. F. DiMauro, *ibid.* **56**, 2590 (1986); G. G. Paulus, W. Nicklich, Huale Xu, P. Lambropoulos, and H. Walther, *ibid.* **72**, 2851 (1994).

[2] A. McPherson, G. Gibson, H. Jara, U. Johann, T. S. Luk, I. A. McIntyre, K. Boyer, and C. K. Rhodes, J. Opt. Soc. Am. B **4**, 595 (1987); M. Ferray, A. L'Huillier, X. F. Li, L. A. Lompre, G. Mainfray, and C. Manus, J. Phys. B **21**, L31 (1988).

[3] P. B. Corkum, Phys. Rev. Lett. **71**, 1994 (1993).

[4] L. V. Keldysh, Sov. Phys. JETP **20**, 1307 (1964); F. H. M. Faisal, J. Phys. B **6**, L89 (1973); H. R. Reiss, Phys. Rev. A **22**, 1786 (1980); Prog. Quantum Electron. **16**, 1 (1992).

[5] M. Lewenstein, K. C. Kulander, K. J. Schafer, and P. H. Bucksbaum, Phys. Rev. A **51**, 1495 (1995).

[6] W. Becker, F. Grasbon, R. Kopold, D. B. Milošević, G. G. Paulus, and H. Walther, Adv. At., Mol., Opt. Phys. **48**, 35 (2001).

[7] D. B. Milošević, G. G. Paulus, D. Bauer, and W. Becker, J. Phys. B **39**, R203 (2006).
[8] H. R. Reiss, Phys. Rev. A **42**, 1476 (1990).
[9] H. R. Reiss, J. Opt. Soc. Am. B **7**, 574 (1990).
[10] D. P. Crawford and H. R. Reiss, Phys. Rev. A **50**, 1844 (1994).
[11] D. P. Crawford and H. Reiss, Opt. Express **2**, 289 (1998).
[12] F. H. M. Faisal and S. Bhattacharyya, Phys. Rev. Lett. **93**, 053002 (2004).
[13] F. H. M. Faisal and T. Radożycki, Phys. Rev. A **47**, 4464 (1993).
[14] A. M. Perelomov, V. S. Popov, and M. V. Terentyev, Zh. Eksp. Teor. Fiz. **50**, 1393 (1966) [Sov. Phys. JETP **23**, 924 (1966)] **51**, 309 (1966) [**24**, 207 (1967)].
[15] V. S. Popov, V. D. Mur, and B. M. Karnakov, JETP Lett. **66**, 229 (1997); Phys. Lett. A **250**, 20 (1998); V. D. Mur, B. M. Karnakov, and V. S. Popov, JETP Lett. **87**, 433 (1998).
[16] V. S. Popov, B. M. Karnakov, and V. D. Mur, JETP Lett. **79**, 262 (2004).
[17] N. Milošević, V. P. Krainov, and T. Brabec, Phys. Rev. Lett. **89**, 193001 (2002); J. Phys. B **35**, 3515 (2002).
[18] H. K. Avetissian, A. G. Markossian, and G. F. Mkrtchian, Phys. Rev. A **64**, 053404 (2001).
[19] V. P. Krainov and S. P. Roshupkin, J. Opt. Soc. Am. B **9**, 1231 (1992).
[20] V. P. Krainov, Opt. Express **2**, 268 (1998); S. P. Goreslavsky and S. V. Popruzhenko, *ibid.* **2**, 271 (1998); V. P. Krainov, J. Phys. B **32**, 1607 (1999); **36**, L169 (2003); V. P. Krainov and A. V. Sofronov, Phys. Rev. A **69**, 015401 (2004).
[21] J. Ortner and V. M. Rylyuk, Phys. Rev. A **61**, 033403 (2000); J. Ortner, J. Phys. B **33**, 383 (2000).
[22] U. W. Rathe, C. H. Keitel, M. Protopapas, and P. L. Knight, J. Phys. B **30**, L531 (1997); S. X. Hu and C. H. Keitel, Phys. Rev. Lett. **83**, 4709 (1999); Phys. Rev. A **63**, 053402 (2001); C. J. Joachain, and N. J. Kylstra, Laser Phys. **11**, 212 (2001); A. Maquet and R. Grobe, J. Mod. Opt. **49**, 2001 (2002); J. S. Roman, L. Roso, and L. Playa, J. Phys. B **36**, 2253 (2003); C. J. Joachain, N. J. Kylstra, and R. M. Potvliege, J. Mod. Opt. **50**, 313 (2003); G. R. Mocken and C. H. Keitel, J. Comput. Phys. **199**, 558 (2004).
[23] M. W. Walser, C. H. Keitel, A. Scrinzi, and T. Brabec, Phys. Rev. Lett. **85**, 5082 (2000).
[24] M. Dammasch, M. Dörr, U. Eichmann, E. Lenz, and W. Sandner, Phys. Rev. A **64**, 061402(R) (2001).
[25] Y. Salamin, S. X. Hu, K. Z. Hatsagortsyan, and C. H. Keitel, Phys. Rep. **427**, 41 (2006).
[26] G. Mocken and C. H. Keitel, J. Phys. B **37**, L275 (2004); C. C. Chirilă, C. J. Joachain, N. J. Kylstra, and R. M. Potvliege, Phys. Rev. Lett. **93**, 243603 (2004).
[27] B. Henrich, K. Z. Hatsagortsyan, and C. H. Keitel, Phys. Rev. Lett. **93**, 013601 (2004).
[28] R. Fischer, M. Lein, and C. H. Keitel, Phys. Rev. Lett. **97**, 143901 (2006).
[29] Q. Lin, S. Li, and W. Becker, Opt. Lett. **31**, 2163 (2006).
[30] N. J. Kylstra, R. A. Worthington, A. Patel, P. L. Knight, J. R. Vázquez de Aldana, and L. Roso, Phys. Rev. Lett. **85**, 1835 (2000).
[31] V. D. Taranukhin, Laser Phys. **10**, 330 (2000); V. D. Taranukhin and N. Yu. Shubin, Quantum Electron. **31**, 179 (2000).
[32] N. Milosevic, P. B. Corkum, and T. Brabec, Phys. Rev. Lett. **92**, 013002 (2004).
[33] C. C. Chirilă, N. J. Kylstra, R. M. Potvliege, and C. J. Joachain, Phys. Rev. A **66**, 063411 (2002).
[34] M. Klaiber, K. Z. Hatsagortsyan, and C. H. Keitel, Phys. Rev. A **74**, 051803(R) (2006).
[35] Y. I. Salamin, Phys. Rev. A **56**, 4910 (1997).
[36] N. J. Kylstra, R. M. Potvliege, and C. J. Joachain, J. Phys. B **34**, L55 (2001).
[37] M. Klaiber, K. Z. Hatsagortsyan, and C. H. Keitel, Phys. Rev. A **71**, 033408 (2005).
[38] D. B. Milošević, S. Hu, and W. Becker, Phys. Rev. A **63**, 011403(R) (2001); Laser Phys. **12**, 389 (2002).
[39] J. D. Bjorken and S. D. Drell, *Relativistic Quantum Mechanics* (McGraw-Hill, New York, 1998), p. 189.
[40] M. Klaiber, K. Z. Hatsagortsyan, and C. H. Keitel, Phys. Rev. A **73**, 053411 (2006).
[41] W. Becker, S. Long, and J. K. McIver, Phys. Rev. A **50**, 1540 (1994).
[42] G. F. Gribakin and M. Yu. Kuchiev, Phys. Rev. A **55**, 3760 (1997).
[43] Y. I. Salamin and F. H. M. Faisal, Phys. Rev. A **54**, 4383 (1996).
[44] T. Brabec and F. Krausz, Rev. Mod. Phys. **72**, 545 (2000); A. L'Huillier, D. Descamps, A. Johansson, J. Norin, J. Mauritsson, and C.-G. Wahlström, Eur. Phys. J. D **26**, 91 (2003); J. Seres, E. Seres, A. J. Verhoef, G. Tempea, C. Streli, P. Wobrauschek, V. Yakovlev, A. Scrinzi, C. Spielmann, and F. Krausz, Nature (London) **433**, 596 (2005).
[45] P. M. Paul, E. S. Toma, P. Breger, G. Mullot, F. Auge, Ph. Balcou, H. G. Muller, and P. Agostini, Science **292**, 1689 (2001); Y. Mairesse, A. de Bohan, L. J. Frasinski, H. Merdji, L. C. Dinu, P. Monchicourt, P. Breger, M. Kovacev, R. Taïeb, B. Carre, H. G. Muller, P. Agostini, and P. Salières, *ibid.* **302**, 1540 (2003); S. A. Aseyev, Y. Ni, L. J. Frasinski, H. G. Muller, and M. J. J. Vrakking, Phys. Rev. Lett. **91**, 223902 (2003); P. Tzallas, D. Charalambidis, N. A. Papadogiannis, K. Witte1, and G. D. Tsakiris, Nature (London) **426**, 267 (2003); R. López-Martens, K. Varjú, P. Johnsson, J. Mauritsson, Y. Mairesse, P. Salières, M. B. Gaarde, K. J. Schafer, A. Persson, S. Svanberg, C. Wahlström, and A. L'Huillier, Phys. Rev. Lett. **94**, 033001 (2005).
[46] N. M. Naumova, J. A. Nees, I. V. Sokolov, B. Hou, and G. A. Mourou, Phys. Rev. Lett. **92**, 063902 (2004); S. Gordienko, A. Pukhov, O. Shorokhov, and T. Baeva, *ibid.* **93**, 115002 (2004).
[47] A. S. Pirozhkov, S. V. Bulanov, T. Zh. Esirkepov, M. Mori, A. Sagisaka, and H. Daido, Phys. Plasmas **13**, 013107 (2006).
[48] http://loa.ensta.fr/Extreme_Light_Infrastructure/EliWeb1.html: Proposal for a European extreme light infrastructure (ELI).